Icarus 218 (2012) 622–643

Contents lists available at SciVerse ScienceDirect

Icarus

journal homepage: www.elsevier.com/locate/icarus

Stability field and phase transition pathways of hydrous ferric sulfates in the temperature range 50 °C to 5 °C: Implication for martian ferric sulfates

Alian Wang [a,*], Zongcheng Ling [a,b], John J. Freeman [a], Weigang Kong [a,c]

[a] Department of Earth and Planetary Sciences, McDonnell Center for Space Sciences, Washington University in St. Louis, St. Louis, MO 63130, USA
[b] School of Space Sciences and Physics, Shandong University, Weihai, Shandong, China
[c] Center for Space Science and Applied Research, Chinese Academy of Sciences, Beijing, China

ARTICLE INFO

Article history:
Received 16 August 2011
Revised 22 December 2011
Accepted 7 January 2012
Available online 28 January 2012

Keywords:
Mars
Mars, Surface
Mineralogy
Spectroscopy
Geological processes

ABSTRACT

We report the results from a systematic laboratory investigation on the fundamental properties of hydrous ferric sulfates. The study involves 150 experiments with duration of over 4 years on the stability field and phase transition pathways under Mars relevant environmental conditions for five ferric sulfates: ferricopiapite [$Fe_{4.67}(SO_4)_6(OH)_2\cdot 20H_2O$], kornelite [$Fe_2(SO_4)_3\cdot 7H_2O$], a crystalline and an amorphous pentahydrated ferric sulfate [$Fe_2(SO_4)_3\cdot 5H_2O$], and rhomboclase [$FeH(SO_4)_2\cdot 4H_2O$]. During the processes of phase transitions, we observed the phenomena that reflect fundamental properties of these species and the occurrence of other common hydrous ferric sulfates, e.g. paracoquimbite [$Fe_2(SO_4)_3\cdot 9H_2O$]. Based on the results of this set of experiments, we have drown the boundaries of deliquescence zone of five hydrous ferric sulfates and estimated the regions of their stability field in temperature (T) – relative humidity (RH) space. Furthermore, we selected the experimental parameters for a next step investigation, which is to determine the location of the phase boundary between two solid ferric sulfates, kornelite [$Fe_2(SO_4)_3\cdot 7H_2O$] and pentahydrated ferric sulfate [$Fe_2(SO_4)_3\cdot 5H_2O$]. The experimental observations in ferricopiapite dehydration processes were used to interpret the observed spectral change of Fe-sulfate-rich subsurface soils on Mars after their exposure by the Spirit rover to current martian atmospheric conditions.

1. Introduction

Martian sulfates record important past and present environmental conditions of the Mars surface and subsurface. The finding of a large amounts sulfates on Mars imply a substantial S-cycling (among gases, liquids, and solids) and that they may have played critical roles for the weathering of surface/subsurface materials, the circulation of metals, and the hydrologic processes in Mars evolution.

Among the martian sulfates, Ca- and Mg-sulfates were observed by orbital remote sensing (by OMEGA instrument on Mars Express and CRISM instrument on Mars Reconnaissance Orbiter, MRO) showing wide distributions and large quantities. Many of these sulfates, especially polyhydrated sulfates, occur in layers that have the thicknesses rarely seen in terrestrial deposits, e.g. 200–400 m thick at Aram Chaos, ~2 km thick at Gale Crater and ~400 m thick at Capri Chasma (Lichtenberg et al., 2009; Milliken et al., 2009; Roach et al., 2009, 2010a, 2010b). The mineralogical details of these thick deposits are worthy of in-depth investigations in future landed missions (MSL and ExoMars). Furthermore, the environmental conditions that enabled such large amount of layered sulfate deposition need to be understood.

In contrast, orbital remote sensing detected Fe-sulfates only in localized areas (Lichtenberg et al., 2010; Milliken and Bish, 2010; Roach et al., 2010b). Nevertheless, Fe-sulfates were identified with more mineralogical detail during the Mars Exploration Rover (MER) missions. Among them, jarosite was identified in Meridiani outcrop (Klingelhofer et al., 2004). A variety of ferric sulfates were found in subsurface salty soils at Gusev (Gellert et al., 2006; Haskin et al., 2005; Johnson et al., 2007; Ming et al., 2008; Morris et al., 2006, 2008; Wang et al., 2006, 2008). More importantly, the dehydration of ferric sulfates was implied on the basis of a set of consecutive Pancam observations that revealed a temporal color changes of the subsurface salty soils from tens of centimeters depth at Tyrone site (near Home Plate, at Gusev) after being excavated and exposed to the martian surface atmospheric conditions (Wang et al., 2008; Wang and Ling, 2011).

The types of hydrous sulfates that we currently see on Mars depend on many factors that include precipitation conditions (brine chemistry, T, pH, EH, RH), the stability field of individual sulfates during Mars climatic evolution (the obliquity changes, seasonal

---

* Corresponding author. Address: Department of Earth and Planetary Sciences, McDonnell Center for Space Sciences, Washington University in St. Louis, One Brookings Drive, St. Louis, MO 63130, USA. Fax: +1 314 935 7361.

E-mail address: alianw@levee.wustl.edu (A. Wang).

0019-1035/$ - see front matter © 2012 Elsevier Inc. All rights reserved.
doi:10.1016/j.icarus.2012.01.003

and diurnal cycles) and the reaction rates of phase transitions. The study of pathways of hydrous sulfate phase transitions and metastable phases are also important because of the slow reaction kinetics in mid-low temperature window at Mars surface and subsurface during the current mid-obliquity period.

Knowledge on the fundamental properties of sulfates, such as stability field, phase transition pathways, reaction rates, can greatly enhance the understanding of mission observations and Mars evolution. There were many recent experimental studies addressing the above properties of Mg- and Ca-sulfates (Chipera and Vaniman, 2007; Chou and Seal, 2003, 2007; Freeman et al., 2007, 2008; Wang et al., 2006, 2009, 2011; Vaniman et al., 2004, 2009; Vaniman and Chipera, 2006), but fewer studies on the properties of Fe-sulfates and especially on ferric sulfates (Chou et al., 2002; Chiper et al., 2007; Hasenmueller and Bish, 2005; Ling and Wang, 2010; Wang et al., 2010; Wang and Ling, 2011; Xu et al., 2009).

In a few early studies (Posnjak and Merwin, 1922; Merwin and Posnjak, 1937; Wirth and Bakke, 1914; Baskerville and Cameron, 1935), the solubility relationships of minerals in the Fe_2O_3–SO_3–H_2O system were investigated in detailed experiments. Posnjak and Merwin (1922) used the quadruple points (i.e. two coexisting solid phases in contact with related solution and vapor) to derive the phase diagram for the Fe_2O_3–SO_3–H_2O system in the 50–200 °C temperature range. Although these high temperature phase relations cannot be directly applied to martian Fe-sulfates, their data provides useful reference points when studying the phase relationships in a temperature range $\leqslant$50 °C.

The goal of our study is to determine the phase relationships of hydrous ferric sulfates in Fe_2O_3–SO_3–H_2O system at Mars relevant temperature range. A temperature range from 50 °C to 5 °C was first studied, in order to produce some results during a reasonable time frame (over 4 years). Experiments at −10 °C which require an even longer time frame have been started; the results will be reported in a later paper.

Different from the work of Posnjak and Merwin (1922) which emphasized the solid–liquid phase boundaries, our study is aimed to study the phase transitions among solid sulfates under current Mars conditions, i.e., the dehydration/rehydration, and chemical reaction after the precipitation of primary ferric sulfates. This investigation was conducted in three phases. First, eight common ferric sulfates were synthesized, with their structures confirmed by X-ray diffraction, and the standard Raman, Vis–NIR (0.4–2.5 μm), and MIR (2.5–25 μm) spectra taken on the same samples (Ling et al., 2008; Ling and Wang, 2010). In the second phase of our investigation, five of these synthesized ferric sulfates were used as the starting phases for a set of 150 experiments to study their stability fields and transition pathways in the T–RH ranges of 5 °C $\leqslant T \leqslant$ 50 °C and 6% $\leqslant$ RH $\leqslant$ 100%. The unique Raman spectra of these sulfates obtained in the first study phase were used for non-invasive phase identification of the intermediate reaction products in second phase. The preliminary results obtained in second study phase (Wang et al., 2010; this study) have provided constraints on the locations of solid–solid phase boundaries among different hydrous ferric sulfates in this $T \sim$ RH space, which are used to design one of the third phase experiments – to determine the phase boundaries between two ferric sulfates: kornelite [$Fe_2(SO_4)_3\cdot 7H_2O$] and pentahydrate ferric sulfate [$Fe_2(SO_4)_3\cdot 5H_2O$] (Kong et al., 2011). We report here, the detail results of second phase of our investigation on five ferric sulfates, and the implication of these results to the martian Fe-sulfates.

Compared with the study of the stability fields and phase transitions of Mg-sulfates (Wang et al., 2006, 2009, 2011), a major complication in the study of ferric sulfates is that there are three types of hydrous ferric sulfates: normal, e.g., $Fe_2(SO_4)_3\cdot 7H_2O$; basic, e.g., $Fe_{4.67}(SO_4)_6(OH)_2\cdot 20H_2O$, and acidic, e.g., $FeH(SO_4)_2\cdot 4H_2O$ (used as starting phases in this study). In addition to the changes in hydration degrees of each type, the possibility of transitions among three types also exists.

2. Samples and experiments

2.1. Samples

Table 1 lists the five synthetic ferric sulfates used as the starting phases in the 150 experiments for stability field and phase transition pathway study. The selection of these five ferric sulfates was based on three criteria: (1) they are reported (or implied) by Mars mission data analysis (e.g., ferricopiapite and rhomboclase); (2) they are commonly observed in terrestrial environments (e.g., ferricopiapite, rhomboclase, pentahydrated ferric sulfate and kornelite); (3) they have the probability of occurrence as suggested by our early experiments (amorphous ferric sulfate, Ling and Wang, 2010).

All five starting phases were synthesized using the method described in Ling and Wang (2010). The chemical purity of synthesized hydrous ferric sulfates was ensured by the pure chemicals used in synthesis procedures. Their crystal structures were confirmed by X-ray diffraction patterns (using PDF2006 database). Their hydration states were confirmed by XRD and Raman, Vis–NIR, and MIR spectroscopy (Ling and Wang, 2010). The hydration state of amorphous ferric sulfate was determined by gravimetric measurements before and after heating it to 200 °C in air for 2 days which produces crystalline anhydrous mikasite (confirmed by XRD and Raman analyses). These gravimetric data indicated that the starting amorphous phase had five structural waters per molecule.

Each starting ferric sulfate sample was re-examined by Raman spectroscopy in which over 100 Raman data points were collected from a flattened ferric sulfate powder sample placed on a glass slide. Consistent Raman spectral patterns and Raman peak positions were obtained from all 100 sampling spots in each of five starting ferric sulfates thus confirming the homogeneity of the composition, structure, and hydration state of each sample.

2.2. Experiments

The humidity buffer technology that we used to study Mg-sulfates (Wang et al., 2006, 2009, 2011) was used again for this study of ferric sulfates. For these experiments, about 100–150 mg ferric sulfate powder was placed in a 12 mm diameter straight-wall glass reaction vial. Each un-capped reaction vial was placed in a 25 mm diameter straight-wall glass bottle that contains RH buffer (a binary salt plus its saturated aqueous solution, based on Chou et al., 2002; Greenspan, 1977). The RH buffer bottle is capped tightly and sealed with Teflon tape. Thirty experiments were conducted for each of the five starting ferric sulfates at three temperatures: 21 ± 1 °C in laboratory ambient, 50 ± 1 °C in an oven and 5 ± 1 °C in a refrigerator. Ten humidity buffers based on saturated aqueous solutions of binary salts were used to give a range of RH's from 6–7% to 100% at each temperature (Table 2). Using a humidity/temperature/dew point meter, we found that the RH uncertainties in our RH buffer bottles were ±1%. The durations of these experiments are between 762 and 1459 days depending on temperatures.

In our experiments at 50 °C and even though the buffer bottles were sealed with Teflon tape and were checked frequently, we still found that in some cases the buffer solutions dried up after weeks in the oven. Due to this reason, we repeated the experiments at 50 °C for all five ferric sulfates. The second set of 50 °C data were shown in figures and tables between 3648 and 18,288 h.

The advantage of humidity buffer technology over that of gas-flow-cell (Chipera et al., 1997; Chou et al., 2002; Xu et al., 2009) is that it can provide stable values of RH and T, the disadvantage

Table 1
Five synthetic hydrous ferric sulfates used for starting materials in the 150 experiments.

Name	Chemical formula	Formation
Rhomboclase	$FeH(SO_4)_2·4H_2O$	Precipitated from Fe–SO_4–H_2O solution
Ferricopiapite	$Fe_{4.67}(SO_4)_6·20H_2O$	Precipitated from Fe–SO_4–H_2O solution
Pentahydrated ferric sulfate	$Fe_2(SO_4)_3·5H_2O$	Baked Am-$Fe_2(SO_4)_3·5H_2O$ at 95 °C and ~10% RH
Kornelite	$Fe_2(SO4)_3·7H_2O$	Baked Am-$Fe_2(SO_4)_3·5H_2O$ at 95 °C and ~60% RH
Pentahydrated amorphous ferric sulfate	$Fe_2(SO_4)_3·5H_2O$	Purchased from ACROS, code 345235000

Table 2
Relative humidity levels at the three temperatures as provided by the saturated aqueous solutions of 10 binary salts used for these experiments (based on Greenspan (1977)).

	5 °C	21 °C	50 °C
LiBr (%)	7	7	6
LiCl (%)	11	11	11
$MgCl_2$ (%)	34	33	31
$Mg(NO_3)_2$ (%)	59	54	45
NaBr (%)	64	59	51
KI (%)	73	70	64
NaCl (%)	76	75	74
KCl (%)	88	85	81
KNO_3 (%)	96	94	85
H_2O (%)	100	100	100

is that if improperly used, it can produce a gradient of RH in the RH buffer bottle. Our experiences suggest a suitable RH buffer should contain more solid binary salt than aqueous solution, with grains of salt exposed to the head-space of buffer bottle. Furthermore, the volume of RH buffer (salt plus solution) should be larger or equal to the volume of head-space. In that way, a roughly balanced RH (±1%) can be maintained in head space of buffer bottle, to react with Fe-sulfates in reaction vial.

2.3. Phase identifications at the intermediate and final stage of experiments

We monitored the progress of the dehydration, rehydration, and phase transitions among normal, basic, and acidic ferric sulfates by non-invasive laser Raman spectroscopic measurements using a HoloLab 5000–532 nm Raman spectrometer by Kaiser Optical Systems, Inc, and by gravimetric measurements using a Mettler PM480 DeltaRange balance. Both measurements were made on the same sample at regular time intervals throughout the entire process (e.g., 2 h, 8 h, 20 h, 48 h, etc. up to 35,016 h). For these measurements, the reaction vial was taken out from the buffer bottle, immediately capped. The mass of whole vial was measured and compared with its initial mass measured prior the starting of experiment. The laser Raman measurement was made on the sample powder, through the glass wall of the sealed reaction vial. In order to monitor the homogeneity of intermediate reaction products, Raman spectra from at least three spots were taken from each sample at each intermediate step. For each of the 30 experiments of a starting phase, an average of 15–24 intermediate stages were taken, thus 7000–9000 pairs of Raman IDs and gravimetric measurements were made for these Fe-sulfates in the entire experiment duration.

The balance (Mettler PM480 DeltaRange) used for gravimetric measurements has an accuracy of ±1 mg. When using 100–150 mg of powder of ferric sulfate as the starting material for each experiment, adding or losing one structural H_2O would cause about 1.5 wt.% mass variations in a ferricopiapite molecule, and 3.4 wt.%, 3.7 wt.%, and 5.6 wt.% in pentahydrate, kornelite, and rhomboclase molecules. For 100–150 mg sample in each experiment, the uncertainty in calculating the number of structural waters held by these molecules based on the gravimetric measurement uncertainty was about $±0.5H_2O$ per ferricopiapite molecular unit to $±0.1H_2O$ per each of other four ferric sulfate molecular unit. These uncertainties are larger than those in the investigation of Mg-sulfates (Wang et al., 2006, 2009, 2011b).

Some of the final products of reactions were selected for powder XRD measurements using a Regaku Geigerflex X-ray diffractometer with a Cu Kα source. Additional mid-IR ATR and NIR diffuse reflectance spectral measurements were made with a Nicolet Nexus670 FTIR spectrometer. No XRD and IR measurements were made on the products of intermediate steps because the gravimetric information would be lost once the sample powder being taken out from the reaction vial for XRD or IR. The descriptions on other details of experimental method can be found in (Wang et al., 2009).

3. Stability field and phase transition pathway of five ferric sulfates

3.1. Ferricopiapite [$Fe_{4.67}(SO_4)_6(OH)_2·20H_2O$]

3.1.1. Structural water in ferricopiapite and structural distortion (quasi-Am) created by vacuum desiccation

The 20 structural waters in a ferricopiapite formula unit (20w in Fig. 1) are in three different types of crystallographic sites. The properties of these sites determine the ease H_2O loss during the dehydration of ferricopiapite. Among the 20 structural waters, six H_2O surround a Fe^{3+} to form [$Fe(OH_2)_6$] octahedra, eight H_2O are in two pairs of [$Fe(OH_2)_2(OH)O_3$] octahedra with each pair interconnected by sharing a common hydroxyl (OH). The remaining six H_2O are not part of any Fe-centered-octahedra, but only linked to the framework by weak hydrogen bonding.

We anticipate these six hydrogen-bonded structural waters to be easily lost during the dehydration of ferricopiapite, while the other 14 H_2O molecules (building blocks of Fe-centered octahedra) would be lost with more difficulty. The structures of Fe-centered octahedra vary in different hydrous Fe-sulfates: [$Fe(OH_2)_6$] and [$Fe(OH_2)_2(OH)O_3$] in ferricopiapite, [$Fe(OH_2)_4O_2$] in rhomboclase (4w in Fig. 1), two types of [$Fe(OH_2)_3O_3$] in kornelite (7w in Fig. 1), [$Fe(OH_2)_3O_3$] and [$Fe(OH_2)_4O_2$] in pentahydrated ferric sulfate (5w in Fig. 1), and [FeO_6], [$Fe(OH_2)_6$], and [$Fe(OH_2)_3O_3$] in paracoquimbite (P9w in Fig. 1). Phase transitions from ferricopiapite to other ferric sulfates therefore require both changes in octahedral configuration and in their connections to [SO_4] tetrahedra. Higher activation energies will be needed in order for these phase transitions to happen.

Nevertheless, the required activation energy is not always available in a temperature range relevant to those at Mars surface, e.g., <25 °C to ~−100 °C at two equatorial exploration region by two Mars Exploration Rovers (Smith et al., 2004, 2006; Spanovich et al., 2006). As observed in laboratory experiments for Mg-sulfates, a sudden removal of structural waters at a moderately low temperature (e.g. <25 °C) can cause the amorphization of the crystal structure of an Mg-sulfate (Vaniman et al., 2004; Wang et al., 2006).

The similar process also occurs in the ferric sulfates. A set of vacuum desiccation experiments were described in Wang and Ling (2011), in which we observed a gradual removal of structural waters from ferricopaipite, accompanied by a distinct change of Raman spectral features. Compared with the Raman spectrum of ferricopiapite (Fig. 2a, there are five groups of peaks below 1400 cm^{-1}: around 1120, 1020, 620, 480, and <300 cm^{-1}), the

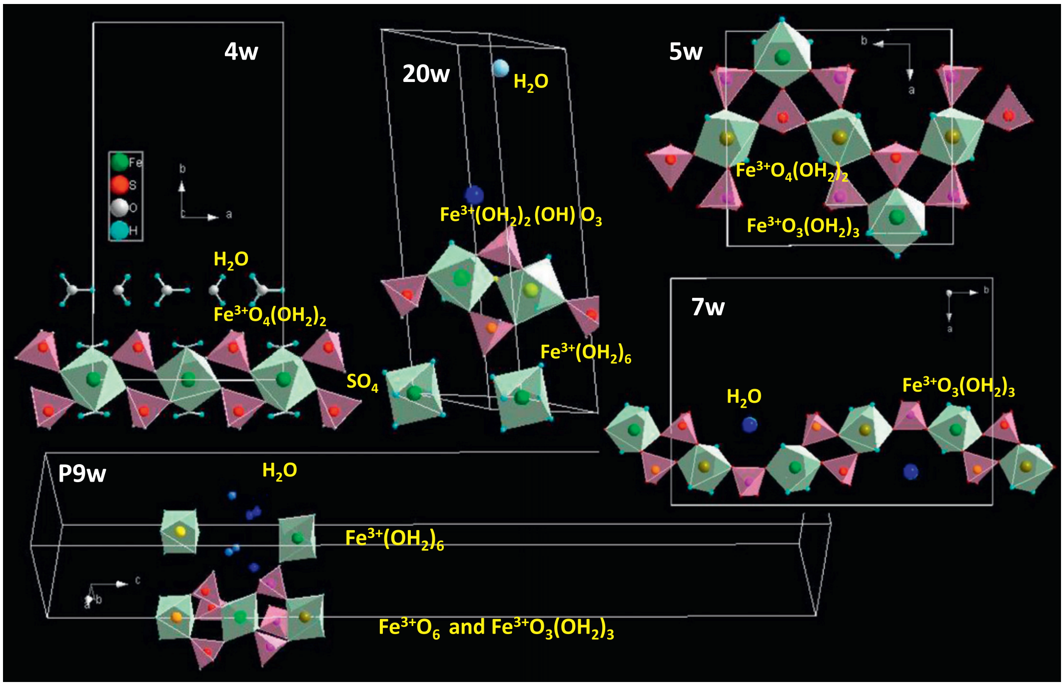

Fig. 1. Details of the basic structural units of rhomboclase (4w), ferricopiapite (20w), lausenite (5w), kornelite (7w), paracoquimbite (p9w). Different types of Fe-centered octahedral sites in these hydrous ferric sulfates were annotated using different colors for the central Fe atoms, from dark green, light green, to yellow. Similarly, different colors (red, pink, orange) were used to mark the central S atom of SO_4 tetrahedra that have non-equivalent crystallographic sites. Dark blue color was used to mark the hydrogen-bonded structural H_2O molecules. (For interpretation of the references to color in this figure legend, the reader is referred to the web version of this article.)

number of peak groups and the relative peak intensities of dehydrated ferricopiapite (Fig. 2b) were basically unchanged (i.e., the basic spectral pattern was retained), but some spectral details were lost (e.g., the doublet near 1020 cm^{-1}), as well as a shift of v_1 Raman spectral peak position (from 1019 to 1023 cm^{-1}) and a broadening of v_1 peak width (from 18 cm^{-1} to 52 cm^{-1}) were observed.

The shifted and broadened of v_1 Raman peak (symmetric stretching vibrational mode of $[SO_4]^{2-}$ tetrahedron) suggest a highly irregular structural environment surrounding each $[SO_4]^{2-}$ tetrahedron, thus a general structural distortion from ferricopiapite had happened. In addition, the XRD patterns of these dehydration products (with 14–19 structural waters per ferricopiapite formula unit) maintains a few XRD lines at similar positions as crystalline ferricopaipite, plus a few additional strong lines (Fig. 19 of Wang and Ling (2011)) and many weak lines with shifted positions, thus supporting a structural distortion. Based on the similar change of its Raman v_1 peak with those observed during the amorphization of Mg-sulfate, we call this dehydrated phase with distorted structure as quasi-amorphous (quasi-Am) in the rest of this manuscript. The second type of amorphous ferric sulfates will be discussed in Section 3.5.4.

The loss of structural H_2O per ferricopiapite formula unit (based on gravimetric measurements) during this vacuum desiccation experiment are shown in Fig. 3. Regardless of the large uncertainties in the plot (discussed in Section 2.3), the general trend of water loss was apparent, and the maximum water loss reached six water molecules per formula unit of ferricopiapite near the end of vacuum desiccation experiment. Based on ferricopiapite crystal structure (20w in Fig. 1), we believe that the water molecules lost during this experiment were the six, interstitial, hydrogen-bonded H_2O molecules. The H_2O molecules that are the building blocks of $[Fe(OH_2)_6]$ and $[FeO_3(OH)(OH_2)_2]$ octahedra were not affected and the end product holds 14 structural H_2O per molecule.

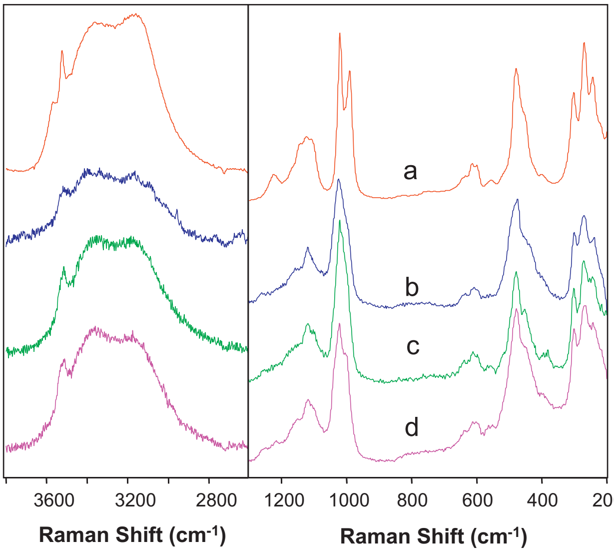

Fig. 2. Raman spectra of ferricopiapite (a), quasi-Am (b) made by fast vacuum desiccation at room temperature, and quasi-Am (c) and UK#09 (d)made by dehydration of ferricopiapite at 6% RH and 50 °C after 20 h and 48 h into the reaction.

3.1.2. Precipitation of ferricopiapite

Our evaporation/precipitation experiments were started from an aqueous solution saturated with $Fe_2(SO_4)_3$ (from $Fe_2(SO_4)_3\cdot 5H_2O$ of ACROS, code 345235000) at room temperature. The dark-brown colored liquid was put into Petri dishes and placed at four temperatures, 50 °C, 21 °C, 5 °C and −10 °C. At 21 °C, the Petri dishes were placed in four humidity buffers (KI, $MgCl_2$, LiCl, and LiBr for RH ~ 73%, 34%, 11%, and 7%, based on Greenspan (1977)). The evaporation and precipitation at other temperatures (50 °C in an oven, 5 °C in a refrigerator and −10 °C in a freezer) were conducted in open air, the corresponding RH values are in the range of <5%, 30–46%, and 60–74% respectively as measured by a temperature/relative humidity sensor placed in the oven, refrigerator, or freezer for several days.

We found that ferricopiapite $[Fe^{3+}_{2/3}Fe^{3+}_4(SO_4)_6(OH)_2 \cdot 20(H_2O)]$ precipitated from all these settings, except at <5% @ 50 °C and $\leqslant$11% @ 21 °C when amorphous ferric sulfate formed. Ferricopiapite is obviously the most common ferric sulfate that precipitates from saturated $Fe^{3+} - SO_4^{2-}$ aqueous solutions (with a Fe:SO$_4$ molar ratio 2:3) under a wide *T* range (50 °C to −10 °C) and a wide RH range (>11%).

3.1.3. Stability field at three temperatures and pathways of dehydration

We conducted the stability field experiments on ferricopiapite at three temperatures (50 °C, 21 °C, 5 °C) and at 10 different RH levels (6–100%) for a period ranging from 18.7 to 48.4 months. The intermediate and the final ferric sulfate phases obtained from these 30 experiments using ferricopiapite as starting phase are shown in Table 3. The changes in the number of structural water per ferricopiapite formula unit calculated based on gravimetric measurements were presented in Fig. 4.

We can see that the deliquescence of ferricopiapite happens when RH $\geqslant$ 75% in the tested temperature range (5–50 °C), and the deliquescence happened directly, i.e., no new solid phases appear before the deliquescence of ferricopiapite.

At 50 °C and RH < 75%, ferricopiapite dehydrates to variety of ferric sulfates. In mid-RH range, ferricopiapite (20w) dehydrates to kornelite (7w) in 65–51% RH and to pentahydrate ferric sulfate (5w) in 45–31% RH. In low-RH range 6–11%, quasi-Am appeared first as the dehydration product (Fig. 2c, very similar to quasi-Am from vacuum desiccation, Fig. 2b), then a new phase (UK#9 in Fig. 2d and Table 3) steadily increases. Gravimetric measurements show a continuous decrease of structural water from 20w to 17w and 14w at these two RH levels. The Raman spectrum of this new phase (Fig. 2d) has finer spectral features than that of quasi-Am (Fig. 2b and c), but is still different from ferricopiapite (Fig. 2a). For example, this new phase has a Raman doublet at 1022 and 1000 cm^{-1} with less separation (Δ = 22 cm^{-1}) than that between the doublet of ferricopiapite at 1019 and 990 cm^{-1} (Fig. 2a, Δ = 29 cm^{-1}). The Raman spectral details imply that UK#9 is a re-crystallized form of quasi-Am, with low (14w–17w) amounts of structural water. Both quasi-Am and UK#9 have less defined OH sites in their structure, as shown as a shifted single wide OH peak at 3514 cm^{-1} (Fig. 2c and d) compared to double OH peaks at 3523 and 3568 cm^{-1} of ferricopiapite (Fig. 2a).

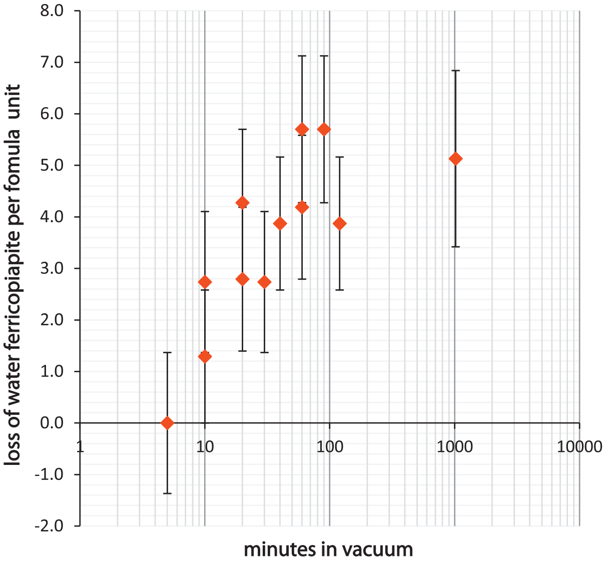

Fig. 3. The number of structural waters per ferricopiapite formula unit that were lost during vacuum desiccation, as calculated from gravimetric measurements. Regardless of the large error bars (due to the relative small mass loss during dehydratioin of ferricopiapite), the plot shows a general trend, which suggests a maximum six structural H_2O per ferricopiapite molecule were lost at the end of this experiment.

These results suggest that the tested RH range (6–100%) at 50 °C does not belong to the stability field of ferricopiapite. The detected remains of ferricopiapite in the final products of experiments at 65–31% RH range apparently are due to the sluggish phase transition from 20w to 7w and to 5w (Table 3). The mixtures of 20w + 7w and 20w + 7w + 5w in the final products caused their apparent 14–20 structural waters seen by gravimetric measurements (Fig. 4c).

The experiments at 21 °C and 5 °C shows that there is a finite RH range (70–54%) where ferricopiapite progressively converts to paracoquimbite ($Fe_2(SO_4)_3{\cdot}9H_2O$) (Table 3, Figs. 4a, b, and 5c). The progress of this conversion seems to develop more steadily at 54% RH and 21 °C. These phenomena indicate that there should be a ferricopiapite–paracoquimbite phase boundary in 54% < RH < 70% and 5 °C < T < 21 °C range. The decreases in mass of the corresponding experimental products are, however, not obvious (Fig. 4a and b) because the end products are mixtures of paracoquimbite and ferricopiapte (Table 3).

Another phase transition, ferricopiapite (20w) to rhomboclase (4w, Table 3, Fig. 5d), was observed at intermediate stages of experiments at mid-low RH values in the 21–5 °C range. It is a dehydration process, in which the H_2O/Fe ratio is reduced from 4.5 to 4 and the $H_2O/(SO_4)$ ratio reduced from 3.5 to 2. However, this phase transition does not show a steady development at every occurrence, i.e. rhomboclase can appear at one or two intermediate stages, and then it can disappear in next few consecutive intermediate stages. We anticipate that the probability of missing the identification of rhomboclase in intermediate stages to be quite low, because (1) Raman peaks of rhomboclase are very distinct from those of ferricopiapite (Fig. 5d and b), and (2) the sample vial was well-shacked before the Raman measurements and at least three spots were checked for each sample at each stage. In addition, the appearance and disappearance of rhomboclase in the intermediate reaction products happened several times (for the experiments 7 < RH < 70% at both 21 °C and 5 °C, Table 3), which suggests that 20w to 4w dehydration is reversible in the tested *T*–RH range. Section 4.2 will give a more detailed discussion on this phase transition. The phase transition from ferricopiapite (20w) to quasi-Am happened only at the lowest RH value (7%) (Table 3), and shows a similar reversibility.

Ferricopiapite remained unchanged (over a period of 48 months) in 73–64% RH at 5 °C. In the ranges of 7% < RH < 34% at 5 °C and 7% < RH < 11% at 21 °C, ferricopiapite converted to UK#9 phase (Fig. 2d), as happened at 50 °C in 6–11% RH, which suggests that another phase boundary should exist in 7% < RH < 33% and the tested *T* range, although we need to wait for the further development of phase equilibrium to determine the involved phases (among ferricopiapite, UK#9, and potentially others).

From above description, we can see the dehydration pathways of ferricopiapite (20w) are: (a) to form 7w, 5w, and UK#9 (through quasi-Am phase) at high *T* ($\geqslant$50 °C); (b) to form paracoquimbite (P9w) in a relatively narrow RH–*T* range (54% < RH < 70% and 5 °C < T < 21 °C); (c) to form UK#9 (with less than 20 structural water) at low RH (33–7%) in mid-low *T* (5–21 °C) range; and (d) through reversible transitions to form rhomboclase (mid RH range) and to quasi-Am (low RH).

3.1.4. Thin film of liquid water at grain surface

The middle two curves in Fig. 4a and b show the development of four experiments (RH = 64% and 73% at 5 °C and RH = 70% and 75% at 21 °C) started with dry powder of ferricopiapite. These gravimetric

Table 3
The intermediate (partial) and the final ferric sulfate phases[a,b] from the 30 experiments starting from ferricopiapite. The phase identifications were made by non-invasive laser Raman measurements.

RH buffer	H_2O	KNO_3	KCl	NaCl	KI	NaBr	$Ma(NO_3)_2$	$MgCl_2$	LiCl	LiBr
T = 50 °C										
RH (%)	100	85	81	74	65	51	45	31	11	6
Time (h)										
2	20w	20w	20w	20w	20w	20w	20w	20w	20w	20w
8	20w,deliq	20w	20w	20w	20w	20w	20w	20w	20w	20w
20	deliq	20w,deliq	20w	20w	20w	20w	20w	20w	Q-am	Q-am
48	deliq	deliq	20w,deliq	20w	20w	20w	20w	20w	20w	UK#9
216	deliq	deliq	20w,deliq	20w	20w,7w	20w	20w	20w	20w	UK#9
384	deliq	deliq	20w,deliq	20w,deliq	20w,7w	20w	20w	20w	20w	UK#9
1080	deliq	deliq	20w,deliq	20w,deliq	20w,7w	20w	20w	20w	UK#9	UK#9
3648	deliq	deliq	deliq	deliq	20w,7w	20w	20w,5w	20w,7w,5w	UK#9	UK#9
13,440	deliq	deliq	deliq	deliq	20w,7w	20w,7w	20w,5w	20w,5w	UK#9,4w	UK#9
T = 21 °C										
RH (%)	100	94	85	75	70	59	54	33	11	7
Time (h)										
2	20w	20w	20w	20w	20w	20w	20w	20w	20w	20w
48	20w,deliq	20w	20w	20w	20w	20w	20w	20w	20w	20w
96	deliq	20w,deliq	Ferri	20w	20w	20w	20w	20w	20w	20w
216	deliq	deliq	20w,deliq	20w	20w	20w	20w	20w	20w	20w
720	deliq	deliq	deliq	20w,deliq	20w	20w	20w	20w	20w	20w
3840	deliq	deliq	deliq	deliq	20w	20w	20w	20w	20w	20w
8664	deliq	deliq	deliq	deliq	20w,4w,UK#4	20w	20w	20w,4w	20w	20w,Q-am
10,488	deliq	deliq	deliq	deliq	20w	20w	20w,P9w	20w,4w	UK#9	UK#9
14,520	deliq	deliq	deliq	deliq	UK#20	20w	20w,P9w	20w	20w	20w
17,688	deliq	deliq	deliq	deliq	20w	20w,7w	20w,P9w	20w	20w,4w	20w
24,912	deliq	deliq	deliq	deliq	20w	P9w,20w	P9w,20w	4w,20w	20w	20w
30,000	deliq	deliq	deliq	deliq	very noisy spec	P9w,20w	P9w,20w	20w	UK#9, 4w	UK#9
34,848	deliq	deliq	deliq	deliq	P9w, 20w	P9w,20w	P9w,20w	20w	UK#9	UK#9
T = 5 °C										
RH (%)	100	96	88	76	73	64	59	34	11	7
Time (h)										
2	20w	20w	20w	20w	20w	20w	20w	20w	20w	20w
96	20w,deliq	20w	20w	20w	20w	20w	20w	20w	20w	20w
216	20w,deliq	20w,deliq	20w	20w	20w	20w	20w	20w	20w	20w
552	deliq	20w,deliq	20w,deliq	20w	20w	20w	20w	20w,4w	20w	20w
720	deliq	deliq	20w,deliq	20w,deliq	20w	20w	20w	20w	20w	20w
2304	deliq	deliq	deliq	20w,deliq	20w	20w	20w	20w	20w,4w	20w
4008	deliq	deliq	deliq	deliq	20w	20w	20w	20w	20w	20w
8736	deliq	deliq	deliq	deliq	20w	20w	20w	20w	20w	20w,Q-am
10,584	deliq	deliq	deliq	deliq	20w	20w	20w	20w	20w	20w
24,960	deliq	deliq	deliq	deliq	20w	20w	P9w,20w	20w	20w	20w,4w
34,848	deliq	deliq	deliq	deliq	20w	20w	P9w,20w	20w, UK#9	20w, UK#9	UK#9

[a] Deliq = deliquescence, 20w = ferricopiapite [$Fe_{4.67}(SO_4)_6(OH)_2 \cdot 20H_2O$], UK#4, 9, 20 = hydrous ferric sulfates with distinct Raman spectra but unknown structures (UK#9 in Fig. 2), 4w = rhomboclase [$FeH(SO_4)_2 \cdot 4H_2O$], Q-am = a Quasi-amorphous phase (details in manuscript), P9w = paracoquimbite [$Fe_2(SO_4)_3 \cdot 9H_2O$].

[b] In the case of multiple phases identified in an intermediate/final product, the one having a higher abundance is listed first in the corresponding cell of above table.

measurements indicate that the H_2O per ferricopiapite molecule increased from 20w to 26.8w and 32.5w (5 °C), or from 20w to 26.4w and 30.9w (21 °C). The Raman spectra obtained from these samples indicate the materials kept a typical ferricopiapite structure evidenced by a distinct spectrum (20w at 5 °C and 73% RH shown as Fig. 5b) from that of Fe^{3+}–SO_4 aqueous solution (deliquescence of 20w at 5 °C and 76% RH shown as Fig. 5a). These observations suggest that the extra H_2O (max ~ 12.5w/molecule at 5 °C, max ~ 10.9w/molecule at 21 °C) must occur at the surface of ferricopiapite grains as adsorbed water. A similar phenomenon was observed in the experiments on epsomite ($MgSO_4 \cdot 7H_2O$) but with much less extra H_2O (Fig. 1 in Wang et al. (2009), a maximum ~0.5 extra H_2O/epsomite molecule at 33% RH and 5 °C). This extra water at the surface of ferricopiapite grain would form layers of liquid water film with considerable thickness. Assuming a closest packing of ferricopiapite molecules in a spherical grain of 10 μm diameter, an extra $12.5H_2O$/ferricopiapite molecule at 5 °C would correspond 2090 layers of H_2O molecules at its surface. By comparison, the extra $0.5H_2O$/epsomite molecule observed at 5 °C would correspond 330 layers of H_2O molecules on the surface of a same size grain.

These experimental data suggest that within a mid-high RH range (65–75%) at 21–5 °C, ferricopiapite grains have the capability to attract many layers of H_2O molecules on their surfaces to form a film of liquid water with a thickness that can be macroscopically observable. Fig. 6a–c shows the photos of a set of samples from these experiments at 5 °C: ferricopiapite equilibrated at 7% RH shown as fine powder with no obvious "extra" H_2O (Fig. 6a); when equilibrated at 64% RH (Fig. 6b), it showed as grain clusters (with extra $6.8H_2O$ per molecule indicated by Fig. 4a); and when equilibrated at 73% RH (Fig. 6c), it showed as paste with shiny surface (with extra $12.5H_2O$ per molecule indicated by Fig. 4a). Note all these samples maintained the characteristic Raman spectrum of ferricopiapite.

3.2. Rhomboclase [$FeH(SO_4)_2 \cdot 4H_2O$]

3.2.1. Precipitation of rhomboclase

When 0.6 g of 98% H_2SO_4 is added to 4 g of saturated $Fe_2^{3+}(SO_4)_3$ solution, rhomboclase [$FeHSO_4)_2 \cdot 4H_2O$] is the major precipitation product (Ling and Wang, 2010). In terrestrial field observations, ferricopiapite would precipitate from a solution with pH 1 to 0, while rhomboclase from pH 0 to −2 (Nordstrom and Alpers, 1999). The precipitation conditions in our experiments are consistent with these field observations.

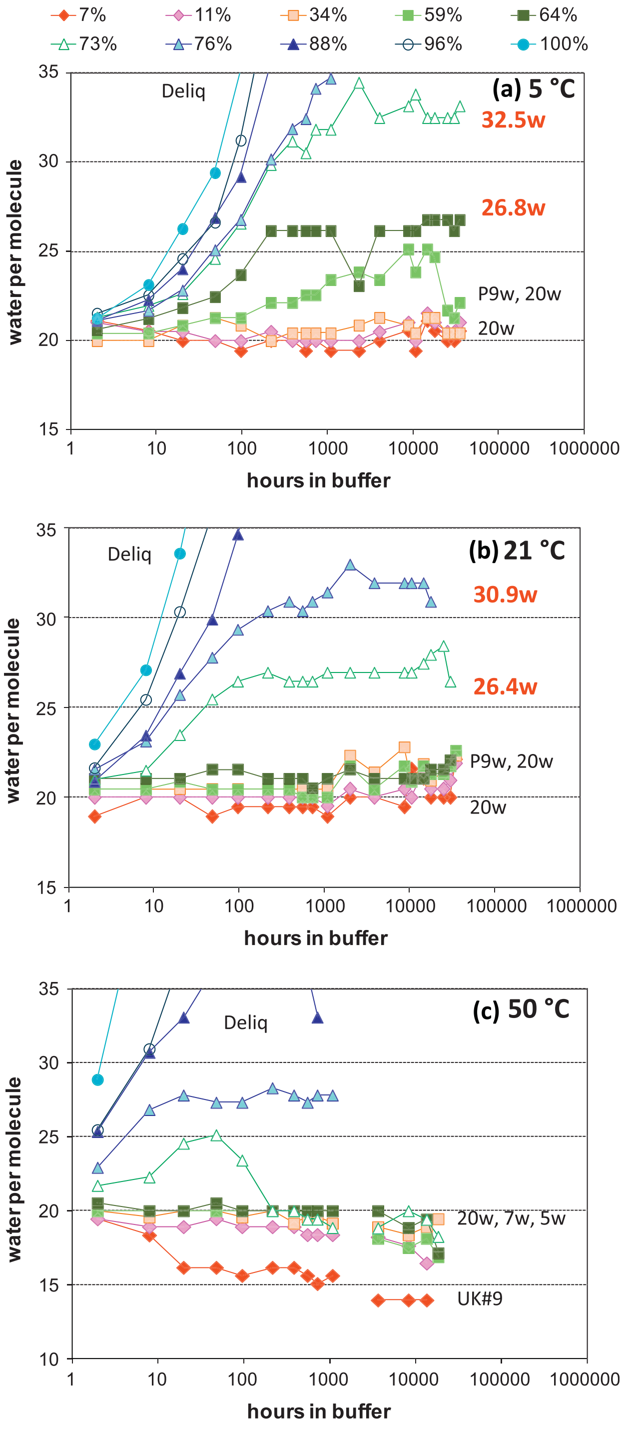

Fig. 4. Changes in the number of structural waters per ferricopiapite formula unit calculated from gravimetric measurements of final and intermediate reaction products of 30 experiments started from ferricopiapite: (a) 5 °C, (b) 21 °C, (c) 50 °C.

In our laboratory experiments (Ling and Wang, 2010; Wang and Ling, 2011, and this study), rhomboclase was never observed to precipitate together with ferricopiapite. Although in principle, the precipitation of ferricopiapite (hydroxyl-bearing) would drive down the pH level of residual solution thus would facilitate the precipitation of hydronium-bearing rhomboclase. Nevertheless, the species like $H_2SO_4^0$, HSO_4^- existing in the residual solution when ferricopiapite is precipitating would lead to a reduced the concentration of H_3O^+, i.e.,

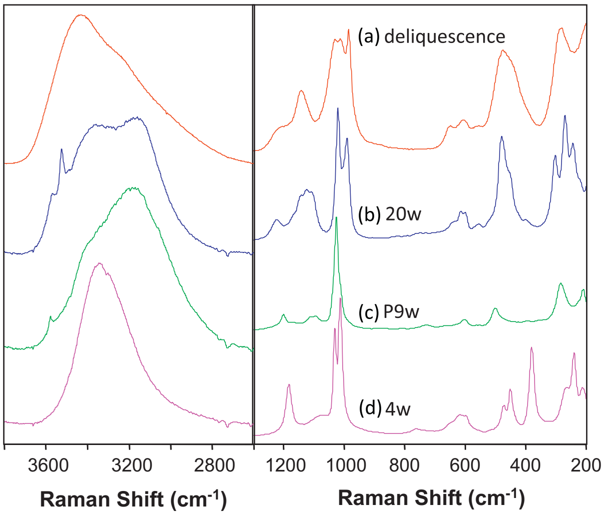

Fig. 5. Raman spectra of (a) $Fe^{3+}{}_2(SO_4)_3$–H_2O solution, (b) ferricopiapite (20w), (c) paracoquimbite (P9w), and (d) rhomboclase (4w).

$$Fe_2(SO_4)_3 + nH_2O \rightarrow Fe^{3+}_{2/3}Fe^{3+}_4(SO_4)_6(OH)_2 \cdot 20(H_2O) \downarrow + H_2SO_4^0 + HSO_4^- + H_3O^+ + SO_4^{2-} + [Fe(OH_2)_6]^{3+} \qquad (4)$$

Therefore, the delayed accumulation of H_3O^+ in the residual solution has delayed the precipitation of rhomboclase. Our observations were that only after the total solidification of precipitated ferricopiapite having been reached, the continuing dehydration will induce the conversion of ferricopiapite to rhomboclase (water/Fe ratio reduces from ~4.5 to 4), as shown in Table 3 and Fig. 6d.

3.2.2. Stability field and the pathway of dehydration and rehydration

We conducted the stability field experiments of rhomboclase at three temperatures (50 °C, 21 °C, 5 °C) and at 10 RH levels (6–100%) for a period of 25.4–48.4 months. The intermediate and the final ferric sulfate phases from these 30 experiments starting from rhomboclase are shown in Table 4. The changes in the number of structural water per rhomboclase formula unit calculated based on gravimetric measurements were presented in Fig. 7.

One can see that the deliquescence of rhomboclase happens in RH ⩾ 65% (50 °C), ⩾70% (21 °C), and ⩾73% (5 °C) (Table 4). The minimum deliquescence RHs for rhomboclase at three tested temperature are all lower than those for ferricopiapite. There are two pathways of deliquescence for rhomboclase: a direct deliquescence at high RH and 50 °C (70–100% RH) to 21 °C (96–100% RH); and an indirect deliquescence through ferricopiapite at mid RH at 50 °C (65% RH) and 5 °C (64–88% RH).

We found that rhomboclase is quite stable at mid-low RH (7% < RH < 64%) over the tested temperature range (5 °C ⩽ T ⩽ 50 °C) with only two exceptions. One exception was at 50 °C and 6% RH (the lowest RH achievable by humidity buffer technology), in which rhomboclase started to dehydrate after 5 months (3648 h, Table 4). The current product of this experiment (after 25 months) is a mixture of rhomboclase and an anhydrous ferric sulfate. The Raman spectrum of this anhydrous phase (UK#19, Fig. 8c) is consistent with its anhydrous nature (no H_2O/OH peak in 4000–2500 cm^{-1}), but different from mikaisite structure (Fig. 8b). The gravimetric measurement (Fig. 7c) indicated that the final product of this experiment has about one H_2O/rhomboclase molecule which is consistent with a mixture of rhomboclase with anhydrous species. The XRD pattern of final product shows lines of rhomboclase plus additional lines at 2θ values of 8.745 and 11.484, but no reasonable match for this phase could be found in X-ray diffraction database PDF2006.

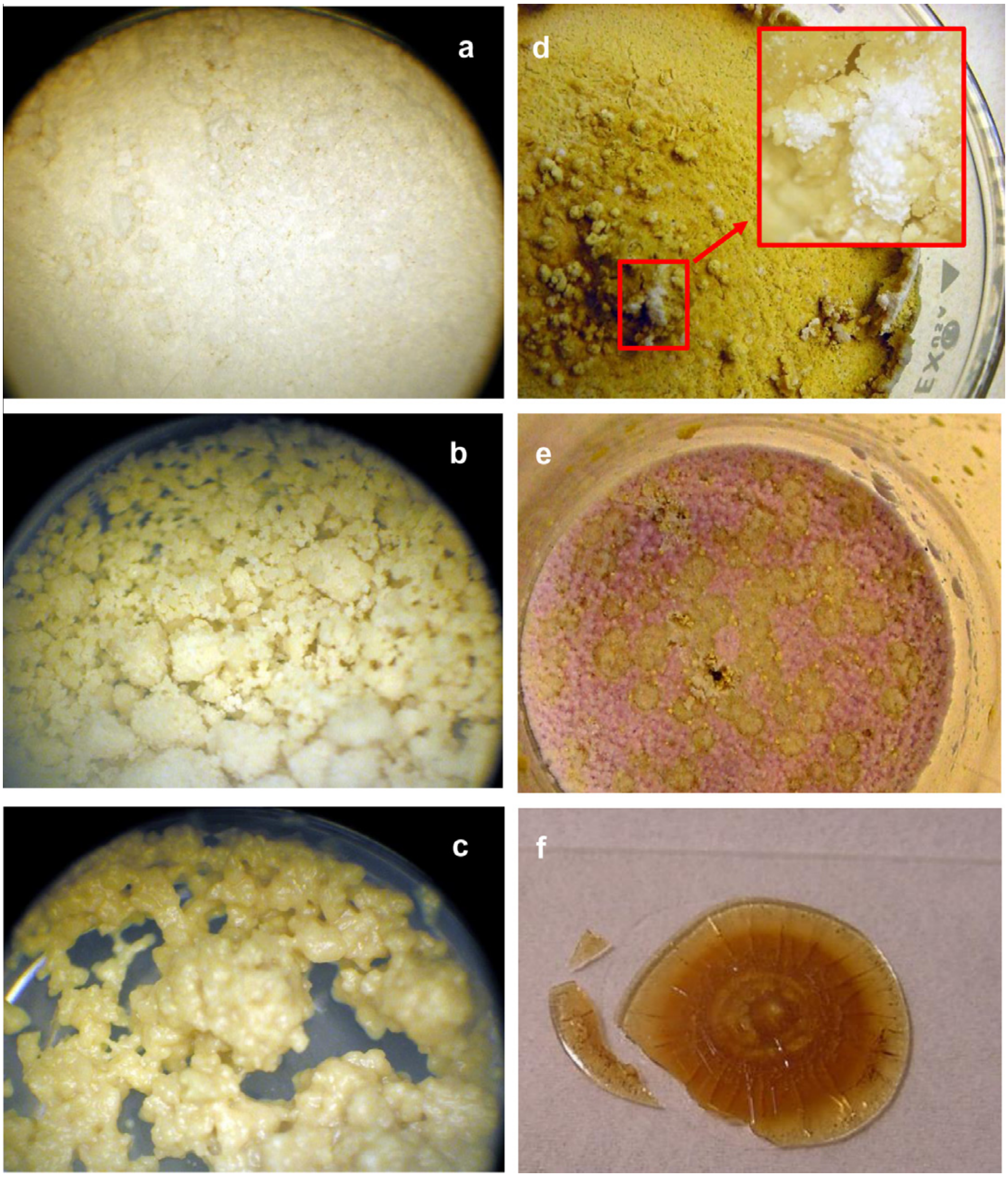

Fig. 6. (a–c) Powder ferricopiapite equilibrated at 5 °C, (a) in 7% RH (LiBr–H_2O buffer); (b) in 64% RH (NaBr–H_2O buffer); (c) in 73% RH (KI–H_2O buffer); (d–f) Precipitation from Fe^{3+}–SO_4–H_2O system, (d) ferricopiapite precipitation at 5 °C and 44% RH, the insert shows rhomboclase grains (white color) produced by ferricopiapite dehydration; (e) mixture of kornelite and rhomboclase precipitated in an oven at 140 °C; (f) amorphous ferric sulfate precipitated 21 °C and 11% RH.

The second exception is the appearance of paracoquimbite in the three experiments in a narrow mid-RH range at 21 °C and 5 °C. At 70% and 59% RH and 21 °C (Table 4), paracoquimbite appeared in a mixture with rhomboclase, and then disappeared. The partial conversion of rhomboclase to paracoquimbite cannot be determined from the gravimetric data (Fig. 7b), probably due to the small mass change. At 64% RH and 5 °C, rhomboclase is first partially converted to ferricopiapite and partially deliquescence, then paracoquimbite appeared and persisted until 48 months into the reaction (Table 4), evidenced by Raman spectroscopy and confirmed by XRD. This phase transition pathway was corroborated by gravimetric measurement (Fig. 7a) where it was found that the number of structural waters increased rapidly from 4w to 15w per rhomboclase molecule (when 4w, 20w, and deliquescence co-exist), then gradually reduced to 11w per rhomboclase, which would correspond about 9.9 structural water based upon the molar mass of paracoquimbite (Fig. 7a at 5 °C). At 59% RH and 5 °C, paracoquimbite appeared after about 25 months into the reaction, and showed a gradual increase of its proportion in the mixture (with 4w) up to 48 months (Table 4). The data of gravimetric measurements (Fig. 7a, 59% RH at 5 °C) show only a gradual mass increase with the final mass corresponding to ~10 waters per rhomboclase molecule. This observation matches with identification of final phases, i.e. a mixture of rhomboclase and paracoquimbite (Table 4).

The conditions where paracoquimbite was observed in the experiments starting with ferricopiapite (Table 4) are 59% RH and 5 °C, 70–54% RH and 21 °C. The observation of paracoquimbite in the experiments starting from rhomboclase under similar *T* and RH conditions (64–59% RH and 5 °C, 59% RH and 21 °C) confirms that a stability field of paracoquimbite exists in this narrow RH–*T* range.

Table 4
The intermediate (partial) and the final ferric sulfate phases[a,b] from the 30 experiments starting from rhomboclase. The phase identifications were made by non-invasive laser Raman measurements.

RH buffer	H_2O	KNO_3	KCl	NaCl	KI	NaBr	$Ma(NO_3)_2$	$MgCl_2$	LiCl	LiBr
T = 50 °C										
RH (%)	100	85	81	74	65	51	45	31	11	6
Time (h)										
2	4w	4w	4w	4w	4w	4w	4w	4w	4w	4w
8	deliq	4w,deliq	4w	4w	4w	4w	4w	4w	4w	4w
20	deliq	deliq	4w,deliq	4w,deliq	4w	4w	4w	4w	4w	4w
48	deliq	deliq	deliq	deliq	4w	4w	4w	4w	4w	4w
216	deliq	deliq	deliq	deliq	7w,20w	4w	4w	4w	4w	4w
552	deliq	deliq	deliq	deliq	7w,20w,deliq	4w	4w	4w	4w	4w
3648	deliq	deliq	deliq	deliq	7w,20w,deliq	4w	4w	4w	4w	4w,UK#19
18,288	deliq	deliq	deliq	deliq	deliq	4w	4w	4w	4w	4w,UK#19
T = 21 °C										
RH (%)	100	94	85	75	70	59	54	33	11	7
Time (h)										
2	4w	4w	4w	4w	4w	4w	4w	4w	4w	4w
20	4w,deliq	4w	4w	4w	4w	4w	4w	4w	4w	4w
96	deliq	deliq	4w,deliq	4w,deliq	4w	4w	4w	4w	4w	4w
216	deliq	deliq	deliq	deliq	4w	4w	4w	4w	4w	4w
384	deliq	deliq	deliq	deliq	4w,deliq	4w	4w	4w	4w	4w
552	deliq	deliq	deliq	deliq	deliq	4w	4w	4w	4w	4w
1992	deliq	deliq	deliq	deliq	P9w,20w,deliq	4w	4w	4w	4w	4w
3840	deliq	deliq	deliq	deliq	deliq	4w	4w	4w	4w	4w
14,520	deliq	deliq	deliq	deliq	deliq	P9w, 4w	4w	4w	4w	4w
17,688	deliq	deliq	deliq	deliq	deliq	4w+	4w	4w	4w	4w
34,848	deliq	deliq	deliq	deliq	deliq	4w+	4w	4w	4w	4w
T = 5 °C										
RH (%)	100	96	88	76	73	64	59	34	11	7
Time (h)										
2	4w	4w	4w	4w	4w	4w	4w	4w	4w	4w
216	4w,deliq	4w	4w	4w,deliq	4w	4w	4w	4w	4w	4w
384	deliq	4w,deliq	4w,deliq	4w,deliq	4w,deliq	4w	4w	4w	4w	4w
552	deliq	deliq	4w,20w,deliq	4w,20w,deliq	4w,deliq	4w	4w	4w	4w	4w
720	deliq	deliq	deliq	deliq	4w,20w,deliq	4w,20w,deliq	4w	4w	4w	4w
4008	deliq	deliq	deliq	deliq	deliq	P9w,20w	4w	4w	4w	4w
24,960	deliq	deliq	deliq	deliq	deliq	P9w,20w	P9w,4w	4w	4w	4w
34,848	deliq	deliq	deliq	deliq	deliq	P9w	P9w	4w	4w	4w

[a] Deliq = deliquescence, 20w = ferricopiapite $[Fe_{4.67}(SO_4)_6(OH)_2\cdot 20H_2O]$, P9w = paracoquimbite $[Fe_2(SO_4)_3\cdot 9H_2O]$, 7w = kornelite $[Fe_2(SO_4)_3\cdot 7H_2O]$, 4w = rhomboclase $[FeH(SO_4)_2\cdot 4H_2O]$, 4w+ = rhomboclase with additional Raman peaks of unknown phase, UK#19 = an anhydrate ferric sulfate with a distinct Raman spectrum (Fig. 8) but unknown structure (details in manuscript).

[b] In the case of multiple phases identified in an intermediate/final product, the one having a higher abundance is listed first in the corresponding cell of above table.

3.3. Kornelite $[Fe_2^{3+}(SO_4)_3\cdot 7H_2O]$

3.3.1. Structural water in kornelite, lausenite, and octahydrated and pentahydrated ferric sulfate

Kornelite structure (Robinson and Fang, 1973) contains layers consisting of a network of $[SO_4]$ tetrahedra and $[Fe(OH_2)_3O_3]$ octahedra perpendicular to c axis (7w in Fig. 1). There are two types of $[Fe(OH_2)_3O_3]$ octahedral in kornelite structure, and each shares three oxygen with three $[SO_4]$ and uses three H_2O as coordinators. With the six structural waters per molecule direct coordinated with Fe^{3+}, the remaining structural water molecules (blue colored H_2O in 7w structure of Fig. 1) occur among the layers, and they are bonded by much weaker hydrogen bonding into the framework.

Different numbers of interlayer structural waters were reported for kornelite. It was reported to be 1.25w by Robinson and Fang (1973), 1.0w by Posnjak and Merwin (1922), and 1.75w by Ackermann et al. (2009). Furthermore, we have found (Ling and Wang, 2010) that this number can be 2.0, i.e. a hydrous ferric sulfate with eight structural waters $[Fe_2(SO_4)_3\cdot 8H_2O]$. It was synthesized from an amorphous pentahydrated ferric sulfate at 95 °C and 30.5% RH (controlled by $MgCl_2$ RH buffer). The product has a XRD pattern quite similar to kornelite, but a very distinct Raman spectral pattern (Fig. 9a). It has a two SO_4 symmetric stretching modes (1037.2 and 1018.2 cm^{-1}), compared with the single peak at 1032.8 cm^{-1} of kornelite (Fig. 9b), two shifted minor peaks at 638 and 452 cm^{-1}, and a broader H_2O band ($\sim$50 cm^{-1} broader than that of kornelite) centered around 3245 cm^{-1}.

When the number of interlayer structural water goes to zero $[Fe_2(SO_4)_3\cdot 6(H_2O)]$, the structure is called lausenite (Robinson and Fang, 1973). The existence of lausenite was questioned by Majzlan et al. (2005), and they reported a crystal structure of pentahydrated ferric sulfate $[Fe_2(SO_4)_3\cdot 5H_2O]$, in which Fe has two octahedral sites with different types of coordinates: $[Fe(OH_2)_3O_3]$, and $[Fe(OH_2)_2O_4]$. Majzlan et al. (2005) argued that this pentahydrated ferric sulfate should be called "lausenite", because they have not found a structure of ferric sulfate with six structural waters. We, however, were able to synthesize both lausenite and a pentahydrated ferric sulfate (Ling and Wang, 2010). We confirmed that our synthesized pentahydrated ferric sulfate has the same XRD pattern as Majzlan et al. (2005) data and a characteristic Raman spectrum shown in Fig. 9d. In addition, we synthesized a hexahydrated ferric sulfate (Ling and Wang, 2010). This hexahydrated ferric sulfate has a pale yellowish color, a distinct XRD pattern with no match in the PDF2006 database, and a distinct Raman spectrum (Fig. 9c) that is different from those of septahydrated $[Fe_2(SO_4)_3\cdot 7H_2O]$ (Fig. 9b), octahydrated $[Fe_2(SO_4)_3\cdot 8H_2O]$ (Fig. 9a), and pentahydrated $[Fe_2^{3+}(SO_4)_3\cdot 5H_2O]$ ferric sulfates (Fig. 9d). More importantly, this phase appeared in the product of one dehydration experiment of kornelite (Table 5, Section 3.3.3), which imply that this phase is an independent hydrous ferric sulfate with its own role in the

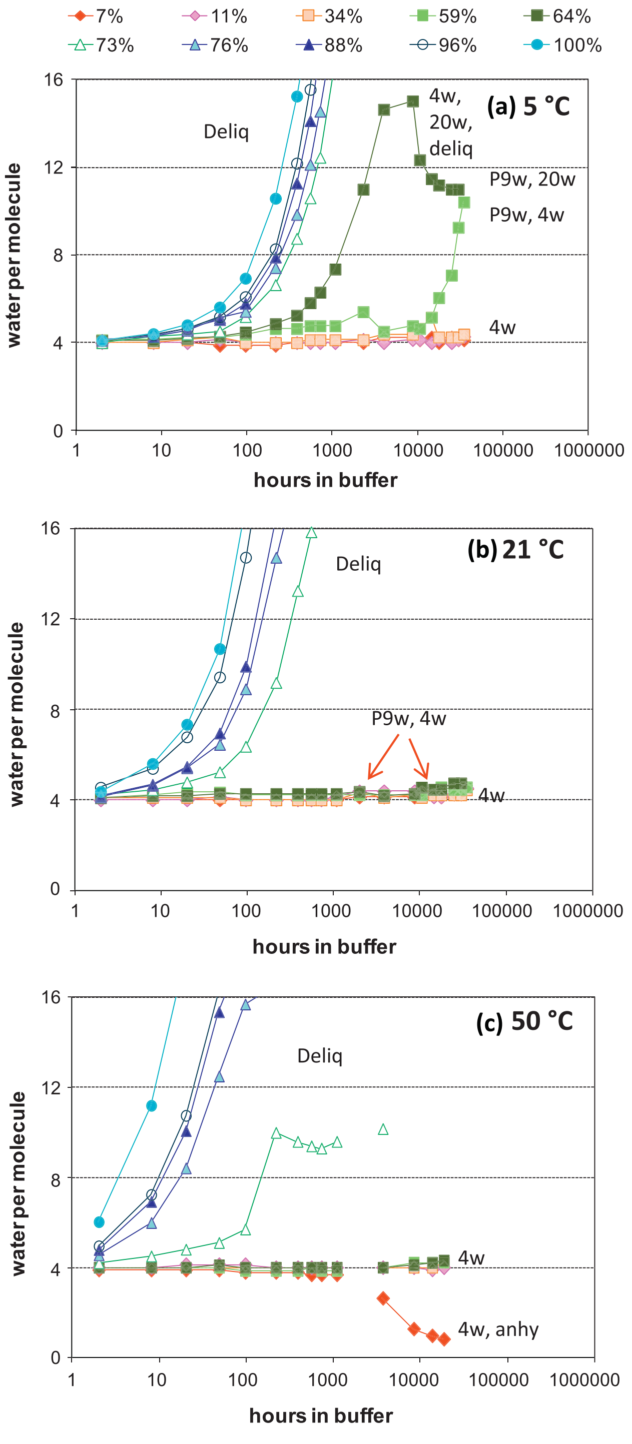

Fig. 7. Changes in the number of structural waters per rhomboclase formula unit calculated from gravimetric measurements of final and intermediate reaction products of 30 experiments started from rhomboclase: (a) 5 °C, (b) 21 °C, (c) 50 °C.

pathways of the phase transitions among other hydrous ferric sulfates. Similarly, octahydrated ferric sulfate, [$Fe_2(SO_4)_3 \cdot 8H_2O$], appeared at several intermediate stages in one experiment (31% RH and 50 °C) started with amorphous [$Fe_2(SO_4)_3 \cdot 5H_2O$] (Table 7).

3.3.2. Precipitation of kornelite

In the full temperature range (50–5 °C) of our experiments, we have not observed the direct precipitation of kornelite [$Fe_2(SO_4)_3 \cdot 7H_2O$] from the aqueous solutions saturated with $Fe^{3+}{}_2(SO_4)_3$. On the other hand, when adding 10 ml of 0.1 m H_2SO_4 into 5 g of an aqueous solution saturated with $Fe_2^{3+}(SO_4)_3$, then heating the mixture to a higher T, e.g., 140 °C, a mixture of kornelite and rhomboclase was precipitated (Fig. 6e). The powdered kornelite sample, used as the starting phase of 30 experiments, was made by baking an amorphous pentahydrated ferric sulfate $Fe_2^{3+}(SO_4)_3 \cdot 5H_2O$ (described in Section 2.1) at 95 °C and ~60% RH (controlled by KI humidity buffer).

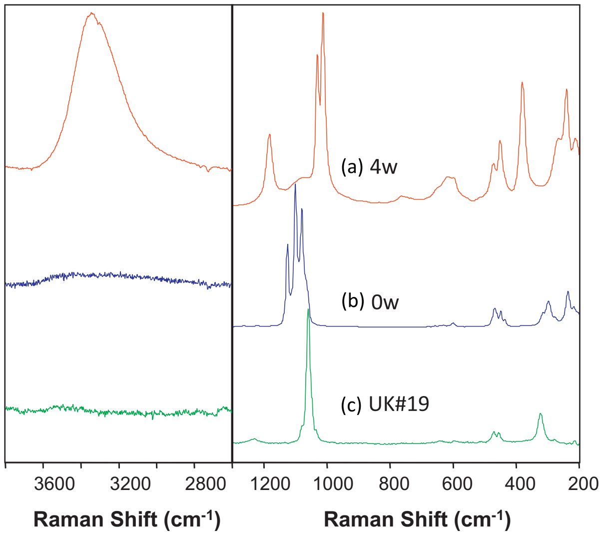

Fig. 8. A comparison of the Raman spectra of (c) an anhydrous ferric sulfate (UK#19) with those of (b) mikasite (0w) and (a) rhomboclase (4w).

3.3.3. Stability field and the pathway of dehydration and rehydration

Thirty experiments started with kornelite [$Fe_2(SO_4)_3 \cdot 7H_2O$] were conducted at three temperatures (50 °C, 21 °C, 5 °C) and at 10 RH levels (6–100%) for a duration of 25.4–48.1 months. The intermediate and the final ferric sulfate phases from these experiments are shown in Table 5. Fig. 10 shows the changes in the number of structural waters per kornelite molecule based on gravimetric measurements of final and intermediate reaction products.

Table 5 shows that the deliquescence of kornelite happens for RH > 74% (50 °C), >70% (21 °C), and >73% (5 °C). More importantly, the direct deliquescence of kornelite was not observed in this tem-

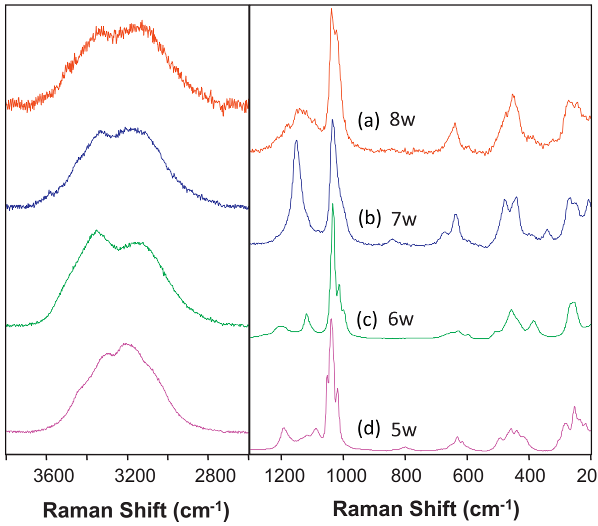

Fig. 9. Characteristic Raman spectra obtained from (a) octahydrated (8w) and (d) pentahydrated ferric sulfates (5w) compared to Raman spectra of (b) kornelite (7w) and (c) lausenite (6w).

perature range. In these experiments, kornelite first rehydrated to ferricopiapite, and then deliquescence occurred (more obviously observed at 21 °C and 5 °C when the deliquescence reaction was slow). This observation means that a phase boundary between kornelite and Fe^{3+}–SO_4-bearing aqueous solution does not exist at $T \leqslant 50$ °C. This conclusion is consistent with the lack of direct precipitation of kornelite (Section 3.3.2) from the aqueous solution saturated with $Fe_2^{3+}(SO_4)_3$ at $T \leqslant 50$ °C.

At 50 °C, with the exception of the four experiments that developed into deliquescence (RH > 74%), we observed a steady phase transition from kornelite to pentahydrated ferric sulfate [$Fe_2(SO_4)_3{\cdot}5H_2O$] at all mid-low RH levels (65–6%, Table 5). Gravimetric measurements (Fig. 10c) indicate a reduction in the number of structural waters from 7w to nearly 4.4w (at 6% RH) and to 6.0w (at 65% RH), which is consistent with the phase ID by Raman spectroscopy (Table 5). These observations imply that kornelite is not a stable phase at this temperature.

At 21 °C and 5 °C (Table 5), kornelite is stable (or metastable) at most RH levels ⩽54% (21 °C), and ⩽34% (5 °C), which is confirmed by gravimetric measurements (Fig. 10a and b).We observed a partial dehydration of kornelite to hexahydrated ferric sulfate [$Fe_2(SO_4)_3{\cdot}6H_2O$, 6w] in an experiment at 7% RH and 5 °C after 888 h h into the reaction (indicated by an arrow in Fig. 10a). Kornelite was the only phase identified in the later stage products (at 2112–34,656 h) of the same experiment, suggesting that it is a more stable phase under these conditions (Table 5).

Similar to the experiments started with ferricopiapite and rhomboclase, during the kornelite dehydration/rehydration experiments, paracoquimbite was observed in a narrow RH range at 21 °C and 5 °C. At 5 °C, it first appeared after 17,520 h into the reaction at 64% and 59% RH, and then became the major phase in the mixture after 24,768 h (Table 5). These phase transitions are confirmed by gravimetric measurements (Fig. 10a), where the number of structural waters per molecule has increased from 7w to 8.4w (at 59% RH) and 9.1w (at 64% RH). At 21 °C, paracoquimbite was only identified at 59% RH level after 14,328 h into the reaction (indicated by an arrow in Fig. 10b), but was not found in three later measurements (up to 34,656 h, Table 5). These observations confirmed the existence of a narrow stability field of paracoquimbite at 21–5 °C and between 65% and 59% RH.

3.4. *Pentahydrated ferric sulfate* [$Fe_2^{3+}(SO_4)\cdot 5H2O$]

3.4.1. *Precipitation*

Similar to kornelite, we have not observed the direct precipitation of pentahydrated ferric sulfate (5w) [$Fe_2(SO_4)_3{\cdot}5H_2O$] from the aqueous solution saturated with $Fe_2^{3+}(SO_4)_3$ in the full temperature range (50–5 °C) of our experiments. The 5w sample for stability study was synthesized by heating the crystalline kornelite at 95 °C under ~10% RH (controlled by LiCl humidity buffer).

Table 5

The intermediate (partial) and the final ferric sulfate phases[a,b] from the 30 experiments starting from kornelite. The phase identifications were made by non-invasive laser Raman measurements.

RH buffer	H_2O	KNO_3	KCl	NaCl	KI	NaBr	$Ma(NO_3)_2$	$MgCl_2$	LiCl	LiBr
T = 50 °C										
RH (%)	100	85	81	74	64	51	45	31	11	6
Time (h)										
2	7w	7w	7w	7w	7w	7w	7w	7w	7w	7w
8	7w,20w,deliq	7w,20w,deliq	7w	7w	7w	7w	7w	7w	7w	7w
20	deliq	deliq	7w	7w	7w	7w	7w	7w	7w	7w
48	deliq	deliq	deliq	7w,20w,deliq	7w	7w	7w	7w	7w	7w
216	deliq	deliq	deliq	deliq	7w	7w	7w	7w	7w	7w
384	deliq	deliq	deliq	deliq	7w	7w	7w	7w	7w,5w	7w,5w
3648	deliq	deliq	deliq	deliq	7w	7w,5w	7w,5w	5w	5w	5w
8256	deliq	deliq	deliq	deliq	7w	5w	5w	5w	5w	5w
18,288	deliq	deliq	deliq	deliq	7w	5w	5w	5w	5w	5w
T = 21 °C										
RH (%)	100	94	85	75	70	59	54	33	11	7
Time (h)										
2	7w	7w	7w	7w	7w	7w	7w	7w	7w	7w
48	7w,20w,deliq	7w,20w,deliq	7w,20w,deliq	7w	7w	7w	7w	7w	7w	7w
72	deliq	7w,20w,deliq	7w,20w,deliq	7w	7w	7w	7w	7w	7w	7w
120	deliq	deliq	7w,20w,deliq	7w,20w,deliq	7w	7w	7w	7w	7w	7w
384	deliq	deliq	deliq	deliq	7w,20w,deliq	7w	7w	7w	7w	7w
3648	deliq	deliq	deliq	deliq	20w	7w	7w	7w	7w	7w
14,328	deliq	deliq	deliq	deliq	deliq	7w,P9w	7w	7w	7w	7w
17,496	deliq	deliq	deliq	deliq	deliq	7w	7w	7w	7w	7w
34,656	deliq	deliq	deliq	deliq	deliq	7w	7w	7w	7w	7w
T = 5 °C										
RH (%)	100	96	88	76	73	64	59	34	11	7
Time (h)										
2	7w	7w	7w	7w	7w	7w	7w	7w	7w	7w
120	7w,20w,deliq	7w,20w,deliq	7w	7w	7w	7w	7w	7w	7w	7w
216	7w,20w,deliq	7w,20w,deliq	7w,20w,deliq	7w,20w,deliq	7w,20w,deliq	7w	7w	7w	7w	7w
384	deliq	7w,20w,deliq	7w,20w,deliq	7w,20w,deliq	7w,20w,deliq	7w	7w	7w	7w	7w
888	deliq	deliq	deliq	7w,20w,deliq	7w,20w,deliq	7w	7w	7w	7w	7w, 6w
2112	deliq	deliq	deliq	deliq	deliq	7w	7w	7w	7w	7w
17,520	deliq	deliq	deliq	deliq	deliq	7w,P9w	7w,P9w	7w	7w	7w
24,768	deliq	deliq	deliq	deliq	deliq	P9w,7w	7w,P9w	7w	7w	7w
34,656	deliq	deliq	deliq	deliq	deliq	P9w	P9w,7w	7w	7w	7w

[a] Deliq = deliquescence, 20w = ferricopiapite [$Fe_{4.67}(SO_4)_6(OH)_2{\cdot}20H_2O$], 7w = kornelite [$Fe_2(SO_4)_3{\cdot}7H_2O$], 5w = [$Fe_2(SO_4)_3{\cdot}5H_2O$], P9w = paracoquimbite [$Fe_2(SO_4)_3{\cdot}9H_2O$], 6w = lausenite [$Fe_2(SO_4)_3{\cdot}6H_2O$], 4w = rhomboclase [$FeH(SO_4)_2{\cdot}4H_2O$].

[b] In the case of multiple phases identified in an intermediate/final product, the one having a higher abundance is listed first in the corresponding cell of above table.

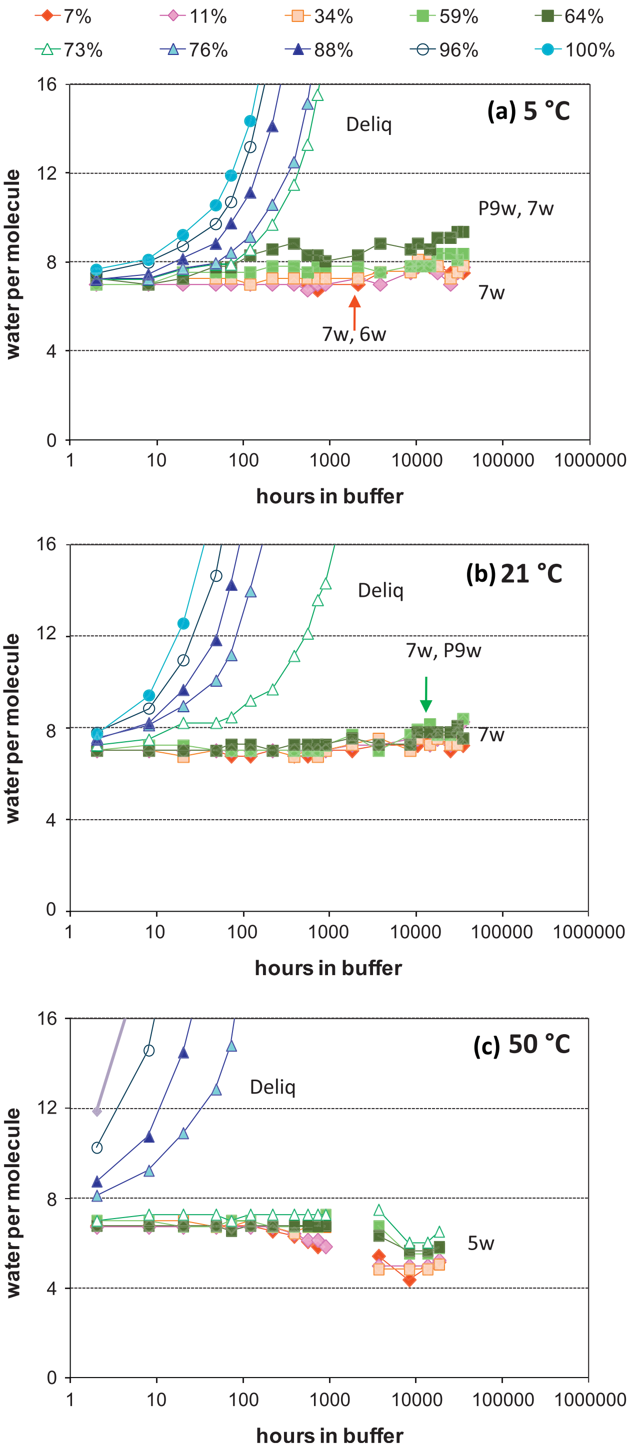

Fig. 10. Changes in the number of structural waters per kornelite formula unit calculated from gravimetric measurements of final and intermediate reaction products of 30 experiments started from kornelite: (a) 5 °C, (b) 21 °C, (c) 50 °C.

3.4.2. Stability field and the pathway of dehydration and rehydration

The 30 experiments started with 5w were conducted at three temperatures (50 °C, 21 °C, 5 °C) and at 10 RH levels (6–100%) for a duration of 25.4–48.1 months. The intermediate and the final ferric sulfate phases from these 30 experiments are shown in Table 6. Fig. 11 shows the changes in the number of structural water per [$Fe_2(SO_4)_3{\cdot}5H_2O$] formula unit calculated from gravimetric measurements of final and intermediate reaction products.

The minimum deliquescence RHs of 5w at 50 °C and 5 °C are the same as for kornelite, but occur at a higher RH ($\geqslant$75%) at 21 °C (Table 6). Another important similarity is that the direct deliquescence of 5w was not observed for all 13 experiments with high RHs. Like kornelite, 5w first rehydrates to ferricopiapite, and then deliquescence occurs. This observation means that a phase boundary between 5w and Fe^{3+}–SO_4-bearing aqueous solution does not exist at $T \leqslant 50$ °C – a conclusion consistent with the observation that direct precipitation of 5w (Section 3.4.1) from the aqueous solution saturated with $Fe_2^{3+}(SO_4)_3$ does not occur at $T \leqslant 50$ °C.

At 50 °C, 5w is stable at all mid to low RH levels (65–6%) (Table 6), as supported by gravimetric data (5.0–5.6w per molecule, Fig. 11c). At 21 °C and 5 °C, it was observed that 5w is stable at all low RH levels $\leqslant$33%. At 21 °C and mid-RH levels (59–54%), 5w converted to a mixture of kornelite and paracoquimbite. At 5 °C, 5w converted to kornelite at 59% RH but to a mixture of ferricopiapite and paracoquimbite at 64% RH. These changes are supported by gravimetric data showing 10w–7.0w at 21 °C and 14w–8.8w at 5 °C respectively for the structural waters per molecule in the final product (Fig. 11a and b).

Similar to the experiments started with ferricopiapite, rhomboclase, and kornelite, the formation of paracoquimbite (from 5w this time) was observed in a narrow RH range (54–59%) at 21 °C and 65% RH at 5 °C.

3.5. Amorphous ferric sulfate [$Fe_2^{3+}(SO_4)_3 \cdot 5H_2O$]

3.5.1. Formation of amorphous phase and its water content

We observed an amorphous (Am) and a quasi-amorphous (quasi-Am) structure in phases derived from ferric sulfates. Quasi-Am (Section 3.1.1, Fig. 2b and c) was formed by rapid dehydration of ferricopiapite, either through vacuum desiccation at room temperature or in an environment of low relative humidity (6–11% RH) and high temperature (50 °C in our experiments, Section 3.1.3). Quasi-Am has a structure distorted from that of ferricopiapite, and can hold 19–14 structural waters per ferricopiapite formula unit.

The amorphous ferric sulfate (Am) was found in the precipitation product (Fig. 6f) from an aqueous solution saturated with $Fe_2^{3+}(SO_4)_3$ at low RH conditions (5–11% RH) and at mid-high temperatures (21 °C and 50 °C in our experiments). The XRD pattern obtained from this material shows no diffraction lines but an elevated background, indicating a non-crystalline structure. Its Raman spectrum is similar to that of quasi-Am in general, but has less detailed spectral features and wide spectral peaks (Fig. 13a). In addition, we found a systematic shift of Raman ν_1 peak position from the precipitated disk of Am in Fig. 6f, at the consecutive spots along a line from its edge to its center). Because the ν_1 Raman peak position of amorphous Mg-sulfate was found to be an indication of their water content (Wang et al., 2006), we anticipate that amorphous ferric sulfates would have a similar property, i.e., to retain different amounts of structural water. This property will be quantified in Section 3.5.3.

3.5.2. A pathway of Am-5w recrystallization

An amorphous ferric sulfate (Am) was used as the starting phase in 30 experiments at three temperatures (50 °C, 21 °C, and 5 °C) and 10 RH levels (6–100%). Powder of this amorphous sample was purchased from ACROS (code 345235000), whose identity and homogeneity were confirmed by XRD and a 100-point Raman measurement. The number of structural waters per $Fe_2(SO_4)_3$ unit in this amorphous phase was determined by gravimetric measurements before and after heating the powder at 200 °C in air for 3 days until it became mikasite – the anhydrous, crystalline $Fe_2^{3+}(SO_4)_3$ (ID was made by XRD and Raman measurements). The gravimetric data confirmed that the original amorphous phase had five structural waters per $Fe_2(SO_4)_3$ formula unit denoted by the abbreviation Am-5w in this manuscript.

Table 6
The intermediate (partial) and the final ferric sulfate phases[a,b] from the 30 experiments starting from pentahydrated ferric sulfate $Fe_2(SO_4)_3{\cdot}5H_2O$. The phase identifications were made by non-invasive laser Raman measurements.

RH buffer	H_2O	KNO_3	KCl	NaCl	KI	NaBr	$Ma(NO_3)_2$	$MgCl_2$	LiCl	LiBr
T = 50 °C										
RH (%)	100	85	81	74	65	51	45	31	11	6
Time (h)										
2	5w	5w	5w	5w	5w	5w	5w	5w	5w	5w
20	deliq	5w,20w,deliq	5w,20w,deliq	5w	5w	5w	5w	5w	5w	5w
48	deliq	5w,20w,deliq	5w,20w,deliq	5w,20w,deliq	5w	5w	5w	5w	5w	5w
72	deliq	deliq	deliq	5w,20w,deliq	5w	5w	5w	5w	5w	5w
216	deliq	deliq	deliq	deliq	5w	5w	5w	5w	5w	5w
18,288	deliq	deliq	deliq	deliq	5w	5w	5w	5w	5w	5w
T = 21 °C										
RH (%)	100	94	85	75	70	59	54	33	11	7
Time (h)										
2	5w	5w	5w	5w	5w	5w	5w	5w	5w	5w
72	deliq	5w,20w,deliq	5w,20w,deliq	5w	5w	5w	5w	5w	5w	5w
216	deliq	deliq	5w,20w,deliq	5w,20w,deliq	5w,20w,deliq	5w	5w	5w	5w	5w
552	deliq	deliq	deliq	20w,deliq	20w,deliq	5w,7w	5w	5w	5w	5w
888	deliq	deliq	deliq	deliq	20w,deliq	5w,7w,20w	5w	5w	5w	5w
1800	deliq	deliq	deliq	deliq	20w,deliq	7w	5w,7w	5w	5w	5w
3648	deliq	deliq	deliq	deliq	deliq	7w	5w	5w	5w	5w
8472	deliq	deliq	deliq	deliq	deliq	7w	5w, 20wt	5w	5w	5w
10,296	deliq	deliq	deliq	deliq	deliq	7w	5w,7w	5w	5w	5w
14,328	deliq	deliq	deliq	deliq	deliq	7w,20w	7w	5w	5w	5w
17,496	deliq	deliq	deliq	deliq	deliq	5w,7w,P9w	5w,7w,P9w	5w	5w	5w
24,696	deliq	deliq	deliq	deliq	deliq	7w,P9w	7w,5w	5w	5w	5w
29,856	deliq	deliq	deliq	deliq	deliq	P9w	7w,4w	5w	5w	5w
34,656	deliq	deliq	deliq	deliq	deliq	P9w	7w, P9w	5w	5w	5w
T = 5 °C										
RH (%)	100	96	88	76	73	64	59	34	11	7
Time (h)										
2	5w	5w	5w	5w	5w	5w	5w	5w	5w	5w
216	5w,20w,deliq	5w,20w,deliq	5w	5w	5w	5w	5w	5w	5w	5w
384	5w,20w,deliq	5w,20w,deliq	5w,20w,deliq	5w,20w,deliq	5w	5w	5w	5w	5w	5w
720	deliq	deliq	5w,20w,deliq	5w,20w,deliq	5w,20w,deliq	5w	5w	5w	5w	5w
888	deliq	deliq	deliq	deliq	5w,20w,deliq	5w	5w	5w	5w	5w
2112	deliq	deliq	deliq	deliq	deliq	7w,5w	7w,5w	5w	5w	5w
3816	deliq	deliq	deliq	deliq	deliq	20w	7w	5w	5w	5w
10,392	deliq	deliq	deliq	deliq	deliq	20w	7w,5w	5w	5w	5w
17,520	deliq	deliq	deliq	deliq	deliq	20w	7w,20w	5w	5w	5w
24,768	deliq	deliq	deliq	deliq	deliq	20w	7w	5w	5w	5w
34,656	deliq	deliq	deliq	deliq	deliq	P9w,20w	7w	5w	5w	5w

[a] Deliq = deliquescence, 20w = ferricopiapite $[Fe_{4.67}(SO_4)_6(OH)_2{\cdot}20H_2O]$, 7w = kornelite $[Fe_2(SO_4)_3{\cdot}7H_2O]$, 5w = $[Fe_2(SO_4)_3{\cdot}5H_2O]$, P9w = paracoquimbite $[Fe_2(SO_4)_3{\cdot}9H_2O]$.

[b] In the case of multiple phases identified in an intermediate/final product, the one having a higher abundance is listed first in the corresponding cell of above table. Trace phase is marked with a "t" at the end of name, e.g., 20 wt.

Table 7 lists the identifications of intermediate and the final ferric sulfate phases by non-invasive Raman measurements from the 30 experiments started with Am-5w, Fig. 12 shows the changes in the number of structural waters per Am-5w formula unit calculated based on gravimetric measurements of final and intermediate reaction products.

Compared with Figs. 4, 7, 10 and 11 (gravimetric data for the experiments started with ferricopiapite, rhomboclase, kornelite, and 5w), the most striking character of Fig. 12 is that for the experiments at mid-RH levels of three temperatures (63–34% RH at 5 °C, 59–33% RH at 21 °C, 65–31% RH at 50 °C), the numbers of structural waters per $Fe_2(SO_4)_3$ formula unit in these intermediate reaction products first increased to certain levels ($18H_2O$/molecule as the maximum), then gradually decreased ($6H_2O$/molecule as the minimum). At 50 °C, the reduction of structural water reached some equilibrium in less than 10 days (73–34% RH); while the equilibria at 5 °C at median RH levels were not reached after 4 years. Referring to the phase transition pathways of Am-5w listed in Table 7, we conclude that the early mass increases were caused by adding water molecules into the non-crystalline structure. The intermediate stages at which the mass decrease started in (Fig. 12) were at about same stages when crystalline species (ferricopiapite, kornelite, and rhomboclase) appeared in the Raman spectra of different experimental products (listed in Table 7). This phenomenon suggests again that an amorphous ferric sulfate structure has the capability of holding variable amounts of structural water.

3.5.3. Number of structural water held by amorphous ferric sulfates

The range of structural waters that can be held by Am structure under a set of defined conditions was evaluated through a set of experiments run at 33.6% RH and 5 °C (Fig. 12a). In these experiments, the amorphous ferric sulfate showed a slow increase of water content, from five to nearly 11 water molecules per $Fe_2(SO_4)_3$ formula unit based on gravimetric measurements (Fig. 12a), accompanied by the appearance of a shift of Raman ν_1 peak position from 1035.1 cm^{-1} to 1020.2 cm^{-1} (Fig. 14). After the ν_1 peak reached 1020 cm^{-1}, the further continuous rehydration induced first the appearance of sharp crystalline Raman peaks of rhomboclase $[FeH(SO_4)_2{\cdot}4H_2O]$ (Fig. 13d, 175–438 days into the reaction), indicating the re-crystallization has started. Ferricopiapite and octahydrated ferric sulfate $[Fe_2(SO_4)_3{\cdot}8H_2O]$ later appear in the experimental products (Fig. 13f and g, 614 and 1040 days). Based on Fig. 14, a rough estimation of water content in the Am structure can be made using their Raman ν_1 peak positions, and the regression line derived from these experimental data has a $R > 0.99$ (Fig. 14, a $R > 0.76$ represents a confident level of 99.9% for 15 data points). In addition,

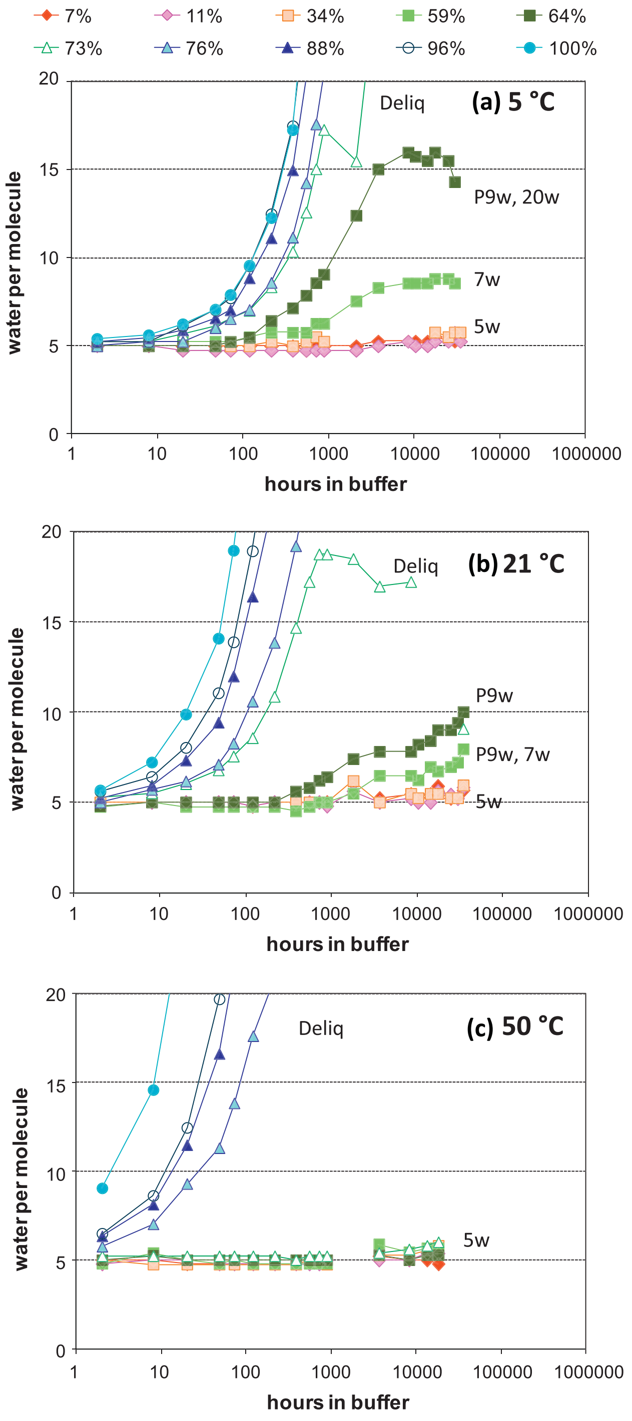

Fig. 11. Changes in the number of structural waters per 5w formula unit calculated from gravimetric measurements of final and intermediate reaction products of 30 experiments started from 5w: (a) 5 °C, (b) 21 °C, (c) 50 °C.

this observation determined the maximum amount of structural water that can be held by Am structure at 5 °C and 33% RH is $11H_2O$ molecules per $Fe_2(SO_4)_3$, i.e., a H_2O to SO_4 ratio of 3.7 that slightly higher than ~3.5 in crystalline ferricopiapite.

The range of Raman ν_1 peak position variation of a distorted ferricopiapite structure (quasi-Am) was much narrower (~4 cm^{-1}) than that of Am (~15 cm^{-1}), signifying the loss of six hydrogen-bounded structural water. This small band shift does not allow a quantitative estimation on the number of structural waters, but the spectral pattern change (Fig. 2b–d) from that of ferricopiapite can serve as an indicator of loss of water and the development of quasi-Am structure.

3.5.4. Am-5w phase transition pathways

Table 7 shows that a different amorphous ferric sulfate would appear before appearance of the deliquescence of Am-5w. The new amorphous phase has a third broad Raman peak in 1300–900 cm^{-1} spectral range (Fig. 13b, c, and abbreviated as Am-3p in this manuscript) where Am-5w has only two broad Raman peaks (Fig. 13a). In addition, Am-3p is the only pathway for Am-5w to re-crystallize to other crystalline hydrous ferric sulfate phases. The XRD patterns of Am-3p and Am-5w are very similar, both are non-crystalline.

As seen in Figs. 2 and 13, ferricopiapite, quasi-Am, Am-5w and Am-3p all have five groups of peaks in their Raman spectra (around 1120, 1020, 620, 480, and <300 cm^{-1}), corresponding the four fundamental vibration modes of $[SO_4]$ tetrahedron (stretching mode ν_1 and ν_3, bending mode ν_2 and ν_4), plus a set of lattice modes at <300 cm^{-1}). The structural distortion in dehydrated ferricopiapite (quasi-Am and UK#9, with loss of up to six hydrogen bonded H_2O per formula unit) caused the disappearance of spectral fine structure in the peak groups near 1120 and 1020 cm^{-1} and the broadening of individual peaks in peak groups near 620, 480, and <300 cm^{-1} (Fig. 2b and c). This change of spectral character is interpreted as a reflection of irregular environment surrounding each $[SO_4]$ tetrahedron, i.e. the lowering in crystallographic site symmetry, without a change of the Fe-centered octahedral symmetry. The Raman spectrum of Am-5w (totally amorphous as seen by XRD) is very different. The five groups of Raman peaks still exist, but the fine structure in the peak groups near 620, 480 and <300 cm^{-1} disappeared and the ν_1 and ν_3 peaks are shifted to higher wavenumbers (near 1036 and 1230 cm^{-1}, Fig. 13a) than those observed in crystalline phases. The difference in the Raman spectrum of Am-3p (from both Am-5w and quasi-Am) is a new peak near 1130 cm^{-1} in between the peaks near 1036 and 1230 cm^{-1} (Fig. 13b and c), accompanied by the decreases in peak width (from ~90 cm^{-1} to ~60 cm^{-1}) and peak position (Fig. 14). In addition, weak and finer spectral structure appear in the peak groups near 620 cm^{-1} and < 300 cm^{-1} of Am-3p. These spectral features suggest a structural ordering surrounding $[SO_4]$ tetrahedra has occurred in Am-3p, which supports that Am-3p to be the pathway of re-crystallization of Am-5w. UK#9 (Fig. 2d) has not only the third peak in between 1036 and 1230 cm^{-1}, it has further a doublet (1022 and 1000 cm^{-1}) which implies a re-crystallization degree higher than Am-3p. The number of structural waters per $Fe_2^{3+}(SO_4)_3$ in UK#9 is slightly lower than Am-3P.

Deliquescence of Am-3p occurs at RH ⩾ 70–75% in the temperature range of 5–50 °C (Table 7). At a low RH level (⩽11%), Am-5w remained unchanged after 4 years into the reactions. Within the mid-RH range, Am-3p re-crystallizes (Fig. 13d–g). The final ferric sulfate phases basically match those phases observed in other 120 experiments with a few exceptions. Due to the starting irregular structure of Am-5w, however, the phase transition pathways are highly variable. Notice octahydrated ferric sulfate $[Fe_2(SO_4)_3{\cdot}8H_2O]$ appeared under mid-RH (30–33%), as the products of early rehydration stages at 50 °C (3–10 days) and 21 °C (54 days), and of later stage at 5 °C (746–1040 days).

4. Discussion

On the basis of the phase identifications reported in Tables 3–7, we can estimate the approximate positions of boundaries of deliquescence zones for the five ferric sulfates of this study. In addition, we can estimate the general locations and expansions of the stability fields for the species that were used as starting phases

Table 7

The intermediate (partial) and the final ferric sulfate phases[a,b] from the 30 experiments starting from amorphous pentahydrated ferric sulfate $Fe_2(SO_4)_3{\cdot}5H_2O$. The phase identifications were made by non-invasive laser Raman measurements.

RH buffer	H_2O	KNO_3	KCl	NaCl	KI	NaBr	$Ma(NO_3)_2$	$MgCl_2$	LiCl	LiBr
T = 50 °C										
RH (%)	100	85	81	74	65	51	45	31	11	6
Time (h)										
2	Am-3p	Am-3p	Am-3p	Am-3p	Am-3p	Am-5w	Am-5w	Am-5w	Am-5w	Am-5w
8	deliq	deliq	20w,deliq	20w,deliq	Am-3p	Am-3p	Am-3p	Am-5w	Am-5w	Am-5w
20	deliq	deliq	deliq	20w,deliq	20w,7w	20w	Am-3p,7w,20w,4w	Am-3p	Am-5w	Am-5w
48	deliq	deliq	deliq	20w,deliq	20w,7w	4w,20w	7 W,20w,4w	Am-3p	Am-5w	Am-5w
72	deliq	deliq	deliq	20w,deliq	20w,7w	20w	7 W,20w,4w	8w,7w	Am-5w	Am-5w
96	deliq	deliq	deliq	20w,deliq	20w,7w	4w,20w	7 W,20w,4w	8w,7w	Am-5w	Am-5w
144	deliq	deliq	deliq	20w,deliq	7w	7 W,20w,4w	7 W,20w,4w	8w,7w	Am-5w	Am-5w
192	deliq	deliq	deliq	20w,deliq	7w	7 W,20w,4w	7 W,4w,UK#14	8w,7w,4w	Am-5w	Am-5w
240	deliq	deliq	deliq	20w,deliq	7w	7 W,20w,4w	7 W,20w,4w	8w,7w,20w	Am-5w	Am-5w
312	deliq	deliq	deliq	20w,deliq	7w	7 W,20w,4w	7 W,20w,4w	7w	Am-5w	Am-5w
432	deliq	deliq	deliq	20w,deliq	7w	20w,4w,7w,5w	7 W,20w,4w	Am-3p,7w,5w	Am-5w	Am-5w
600	deliq	deliq	deliq	20w,deliq	7w	7 W,20w,4w	7 W,20w,4w	7w,5w,4w	Am-5w	Am-5w
792	deliq	deliq	deliq	20w,deliq	7w	7 W,20w,4w	7 W,20w,4w	5w	Am-5w	Am-5w
936	deliq	deliq	deliq	20w,deliq	7w,P9w,20w	7 W,20w,4w	7w,20w	5w	Am-5w	Am-5w
1296	deliq	deliq	deliq	20w,deliq	7w	7 W,20w,4w	7w,20w	5w,4w	Am-5w	Am-5w
2208	deliq	deliq	deliq	20w,deliq	7w	7w	7w	5w	Am-5w	Am-5w
8256	deliq	deliq	deliq	deliq	7w	7w	7w,5w,6w	5w	5w,6w	Am-5w
18,288	deliq	deliq	deliq	deliq	7w,5w	7w	5w	5w	5w	Am-5w
T = 21 °C										
RH (%)	100	94	85	75	70	59	54	33	11	7
Time (h)										
2	Am-3p	Am-5w	Am-5w	Am-5w	Am-5w	Am-5w	Am-5w	Am-5w	Am-5w	Am-5w
8	Am-3p	Am-3p	Am-3p	Am-3p	Am-5w	Am-5w	Am-5w	Am-5w	Am-5w	Am-5w
20	Am-3p	Am,deliq	Am,deliq	Am,deliq	Am-3p	Am-3p	Am-3p	Am-5w	Am-5w	Am-5w
48	deliq	deliq	20w,deliq	20w,deliq	Am-3p	Am-3p	Am-3p	Am-3p	Am-5w	Am-5w
72	deliq	deliq	deliq	20w,deliq	20w	Am-3p	Am-3p	Am-3p	Am-5w	Am-5w
96	deliq	deliq	deliq	20w,deliq	20w	Am,Ferric	Am-3p,20w,4w	Am-3p	Am-5w	Am-5w
144	deliq	deliq	deliq	20w,deliq	20w	20w	7w,20w,4w,UK#14	Am-3p	Am-5w	Am-5w
192	deliq	deliq	deliq	20w,deliq	20w	20w	4w,20w	Am-3p	Am-5w	Am-5w
240	deliq	deliq	deliq	20w,deliq	20w	20w	20w	Am-3p	Am-5w	Am-5w
312	deliq	deliq	deliq	20w,deliq	20w	20w	4w,20w	Am-3p	Am-5w,Am-3p	Am-5w
432	deliq	deliq	deliq	20w,deliq	20w	20w	20w	Am-3p	Am-5w	Am-5w
600	deliq	deliq	deliq	20w,deliq	20w	20w	4w,20w+	UK#9	Am-5w	Am-5w
792	deliq	deliq	deliq	20w,deliq	20w,deliq	20w	4w,20w	UK#14, UK#13	Am-5w	Am-5w
936	deliq	deliq	deliq	20w,deliq	20w,deliq	20w,7w	4w,20w	UK#17	Am-5w	Am-5w
1296	deliq	deliq	deliq	20w,deliq	20w,deliq	20w,P9w,7w	20w,7w,4w	4w,20w,8w	Am-5w	Am-5w
2184	deliq	deliq	deliq	20w,deliq	20w,deliq	20w,deliq	4w	UK#9	Am-5w	Am-5w
4032	deliq	deliq	deliq	20w,deliq	20w,deliq	7w	5w	4w	Am-5w	Am-5w
8856	deliq	deliq	deliq	deliq	20w,deliq	Am,20w,P9w	20w,4w	Am-3p	Am-5w	Am-5w
10,680	deliq	deliq	deliq	deliq	20w,deliq	20w	4w	4w,7w,20w	7w,5w,20w	P9w
14,712	deliq	deliq	deliq	deliq	deliq	20w	P9w	20w	Am-5w	Am-5w
17,880	deliq	deliq	deliq	deliq	deliq	7w,P9w	20w,4w,7w	20w,4w,7w	4w,7w	P9w,7w
25,032	deliq	deliq	deliq	deliq	deliq	P9w,7w,20w	P9w,7w	4w,7w,20w	4w	7w
30,144	deliq	deliq	deliq	deliq	deliq	P9w,7w,	P9w,4w,20w	7w,UK#9,20w	7w,20w,4w	P9w,7w,4w
35,016	deliq	deliq	deliq	deliq	deliq	P9w	P9w,7w	7w,4w	P9w,4w	7w
T = 5 °C										
RH (%)	100	96	88	76	73	64	59	34	11	7
Time (h)										
2	Am-5w	Am-5w	Am-5w	Am-5w	Am-5w	Am-5w	Am-5w	Am-5w	Am-5w	Am-5w
20	Am-3p	Am-5w	Am-5w	Am-5w	Am-5w	Am-5w	Am-5w	Am-5w	Am-5w	Am-5w
48	deliq	Am-3p	Am-3p	Am-3p	Am-3p	Am-5w	Am-5w	Am-5w	Am-5w	Am-5w
72	deliq	deliq	deliq	Am-3p	Am-3p	Am-3p	Am-3p	Am-5w	Am-5w	Am-5w
240	deliq	deliq	deliq	20w,deliq	20w,deliq	Am-3p,20w	Am-3p	Am-5w	Am-5w	Am-5w
312	deliq	deliq	deliq	20w,deliq	20w,deliq	20w	Am-3p	Am-5w	Am-5w	Am-5w
432	deliq	deliq	deliq	20w,deliq	20w,deliq	20w	20w	Am-3p	Am-5w	Am-5w
4200	deliq	deliq	deliq	20w,deliq	20w,deliq	20w	20w	4w,20w	Am-5w	Am-5w
8928	deliq	deliq	deliq	deliq	20w,deliq	20w	P9w	Am-3p,4w	Am-5w	Am-5w
10,776	deliq	deliq	deliq	deliq	deliq	20w	P9w	Am-3p,4w,20w	Am-5w	Am-5w
17,904	deliq	deliq	deliq	deliq	deliq	20w	P9w	UK#9,8w,4w	Am-5w	Am-5w
25,152	deliq	deliq	deliq	deliq	deliq	20w	P9w	UK#9,8w,4w	Am-5w	Am-5w
30,144	deliq	deliq	deliq	deliq	deliq	P9w,UK#23	P9w	20w,7w,4w	Am-5w	Am-5w
35,016	deliq	deliq	deliq	deliq	deliq	P9w,UK#23	P9w	7w,4w	Am-5w	Am-5w

[a] Deliq = deliquescence, Am-5w = amorphous [$Fe_2(SO_4)_3{\cdot}5H_2O$], Am-3p = amorphous ferric sulfate with 3 Raman peaks in 1300–1000 cm^{-1}, 20w = ferricopiapite [$Fe_{4.67}(SO_4)_6(OH)_2{\cdot}20H_2O$], P9w = paracoquimbite [$Fe_2(SO_4)_3{\cdot}9H_2O$], 8w = [$Fe_2(SO_4)_3{\cdot}8H_2O$], 7w = kornelite [$Fe_2(SO_4)_3{\cdot}7H_2O$], 6w = [$Fe_2(SO_4)_3{\cdot}6H_2O$], 5w = [$Fe_2(SO_4)_3{\cdot}5H_2O$], 4w = rhomboclase [$FeH(SO_4)_2{\cdot}4H_2O$], UK#9, 13, 14, 23 = hydrous ferric sulfates with distinct Raman spectra but unknown structures.

[b] In the case of multiple phases identified in an intermediate/final product, the one having a higher abundance is listed first in the corresponding cell of above table.

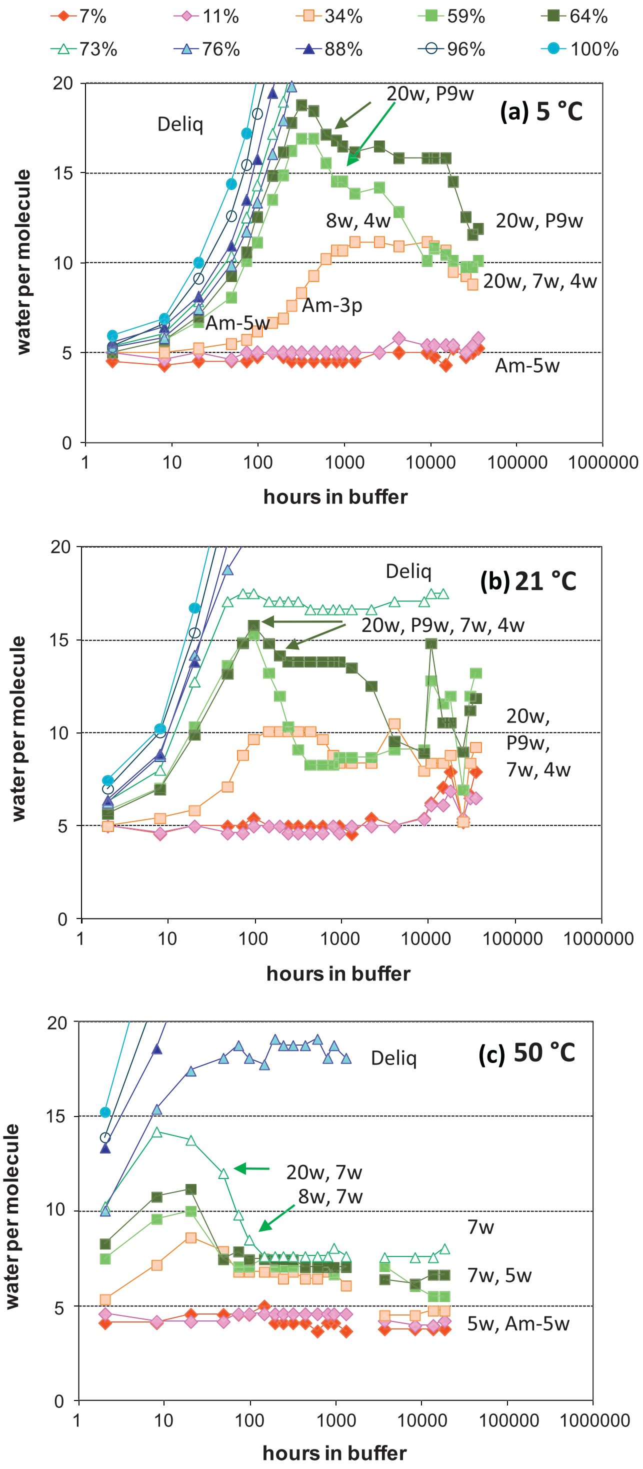

Fig. 12. Changes in the number of structural waters per Am-5w formula unit calculated from gravimetric measurements of final and intermediate reaction products of 30 experiments started from Am-5w: (a) 5 °C, (b) 21 °C, (c) 50 °C.

and that appeared frequently (e.g. paracoquimbite) in these experiments.

4.1. Zones of deliquescence

Because these experiments in this study were designed to find the approximate locations of the stability fields for the ferric sulfates, 10 discrete RH levels were used at each of the three temperatures, therefore only a *range* (instead of a value) of RH will be determined when estimating the boundary of deliquescence zones. For example, we observed the deliquescence of ferricopiapite at 76% RH at 5 °C, while ferricopiapite remains unchanged at 73% RH at 5 °C. Thus the RH range of 73–76% would be the estimated boundary of deliquescence zone at 5 °C for ferricopiapite. Connecting the three RH ranges at three tested temperatures, the estimated boundary of deliquescence zone for each ferric sulfate species would be a thick line or a “band” that goes through a space in *T*–RH field.

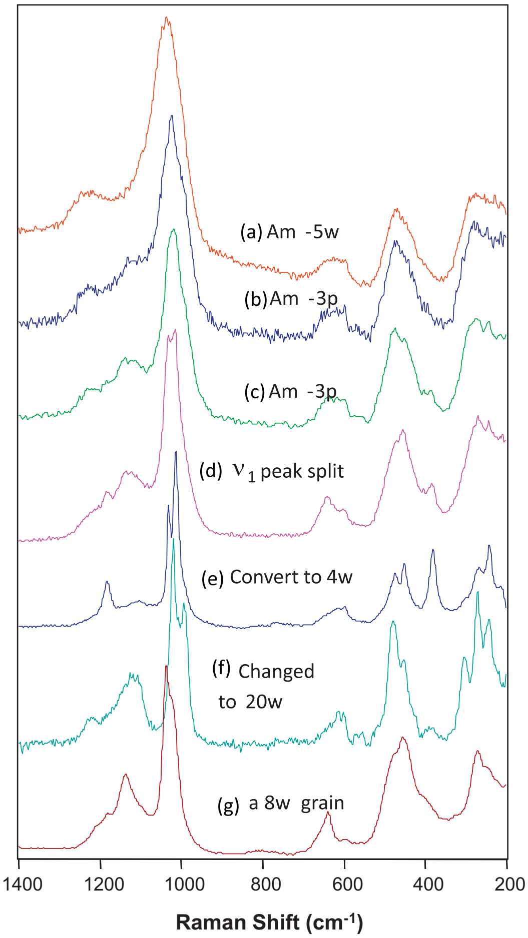

Fig. 13. The changes in Raman peak shape during a rehydration experiment of Am-5w at 5 °C in $MgCl_2$ buffer (33% RH). (a) Am-5w after 1 day in RH buffer; (b and c) after 18 days (and 104 days) into reaction, Am-3p phase appeared with a third peak (~1130 cm^{-1}) between the two major peaks of Am-5w near 1230 and 1036 cm^{-1}, accompanied by the decreases in the width (from 90 cm^{-1} to ~60 cm^{-1}) and the position of near 1036 cm^{-1} peak; (d) A splitting of ν_1 peak appeared at 175 days, with further reduction of peak width (~ 46 cm^{-1}); (e–g) the characteristic Raman peaks of rhomboclase (4w, after 449 days), ferricopiapite (20w, after 613 days), and octahydrated ferric sulfate (8w, after 1048 days) all appeared at the later stages of re-crystallization.

The estimated boundaries of deliquescence zones of ferricopiapite, rhomboclase, and 7w/5w/Am, were drawn in Fig. 15 (as blue colored, green colored and red colored straight thick lines). Since we have found (Sections 3.3.2 And 3.4.2) that ferricopiapite was the necessary pathway in the deliquescence process of both 7w and 5w, the boundary location of 5w/7w – deliquescence (red colored thick line) would show the *T*–RH region in which 5w or 7w can keep their structural framework, and should be considered as the location of 5w/7w – ferricopiapite – deliquescence boundary. The fact of this boundary occurs at lower RH side of ferricopiapite – deliquescence boundary at 21 °C to 5 °C, suggests that 7w, 5w, and Am have a narrow RH stability field at mid-low T, compared with ferricopiapite.

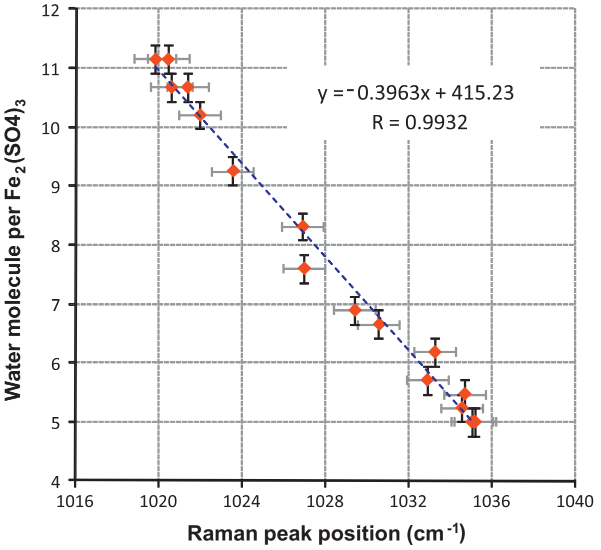

Fig. 14. Raman peak position shifts during a rehydration process of Am-5w at 34% RH and 5 °C. The regression line shows a tight correlation ($R > 0.99$) between the Raman peak position (cm^{-1}) and the number of structural water per $Fe_2(SO_4)_3$ molecule, determined by gravimetric measurements. Notice a $R > 0.76$ would represent a confident level of 99.9% for 15 data points.

Similarly, the rhomboclase – deliquescence boundary occurs at lower RH side of ferricopiapite – deliquescence boundary in full tested *T* range (5–50 °C), which suggests a narrower RH stability field of rhomboclase than that of ferricopiapite.

Although the uncertainties in the exact locations of these estimated boundaries would be large (±1/2ΔRH between two buffered RH values), the differences in the locations of these boundaries are nevertheless very reliable, as they were built on the basis of phase ID(s) in the experiments with >2–4 years duration (Tables 3–7). For example, the location of ferricopiapite – deliquescence boundary is in the range of 73–75% RH at 5 °C, 70–75% RH at 21 °C and 65–74% RH at 50 °C, whereas rhomboclase – deliquescence boundary is in the range of 64–73% RH at 5 °C, 59–70% RH at 21 °C and 51–65% RH at 50 °C. When RH increases, therefore, the deliquescence of rhomboclase would occurs earlier than ferricopiapite at all *T*.

4.2. Stable and metastable fields

On the basis of the phase ID reported in Tables 3–7, we can estimate the general locations and expansions of the stability fields for the starting ferric sulfates and those that appeared during our experiments. The variations in reactions rates at different temperatures can bring uncertainty, i.e., the slow rates of certain reactions can cause the lack of equilibrium even after up to 4 years (the maximum duration of our laboratory experiments).

Using pentahydrated ferric sulfate [$Fe_2(SO_4)_3{\cdot}5H_2O$, 5w] as an example (Fig. 15a). We are confident that RH range 6–61% at 50 °C is within its stability field, because: (1) 5w stays as 5w, and 7w converted into 5w within this *T*–RH range after one year (Tables 5 and 6); (2) at 50 °C and at several RH levels, ferricopiapite and Am-5w converted into 5w (Tables 3 and 7); and especially (3) we have determined the exact location of 5w–7w phase boundary to be at 60.7% RH at 50 °C (Kong et al., 2011), using a much more precise experimental method (continuously changing the *T* and RH in a small zone) and a set of experimental parameters based on the results of this study. The 5w–7w phase boundary is plotted in Fig. 15a (a solid black line between two experimental determined points from 35.8 °C to 56.2 °C). In contrast, we are not so confident if the range of 7–33% RH and 5–21 °C is part of stability field of 5w. Although we have observed the persistence of 5w in this RH–*T* range, we also observed the persistence of kornelite (7w), rhomboclase (4w), and ferricopiapite (20w) up to 4 years into the experiments in these *T* and RH ranges. On the basis of these observations, we can only say that an area in this region may be part of stability field of 5w and that the exact locations of its boundaries to other species need to be determined by more experiments. For this reason, we used the shades of color in Fig. 15 to present the confidence levels of our study on the different parts of stability field. For example, a dense purple shade (high confidence) was used in the zone of 6–65% RH and 50 °C for the stability field of 5w, a light purple shade (less confidence) was used for

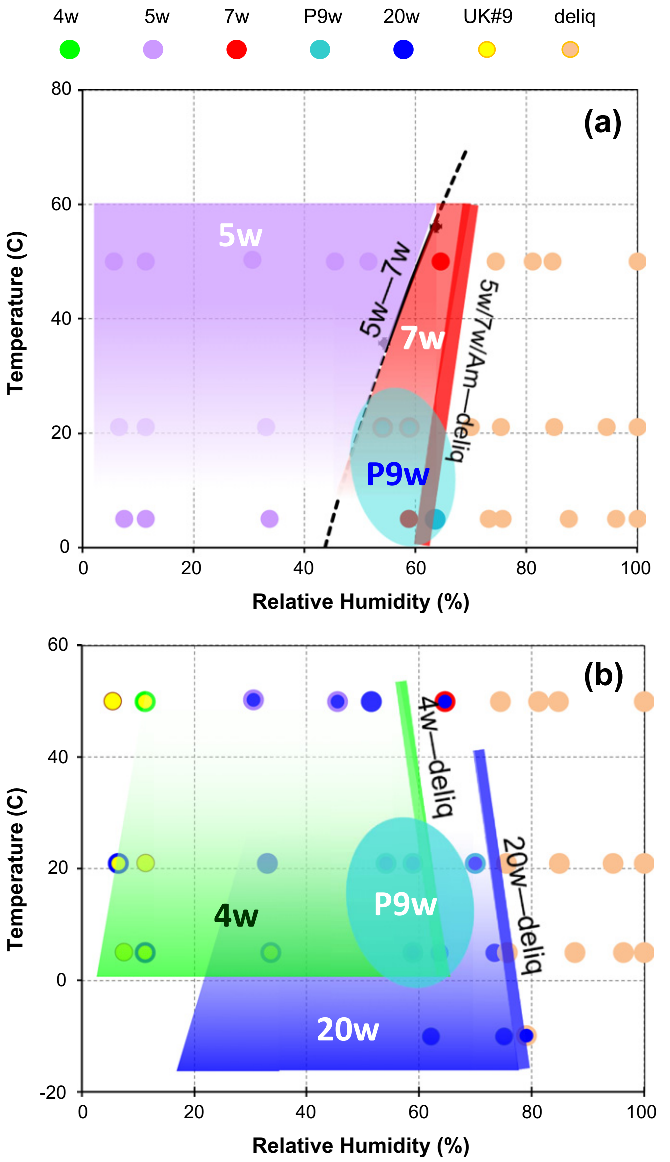

Fig. 15. (a) Stability and metastability fields of 5w, 7w, and P9w, plot on the base of final phases of experiments starting with 5w. The darker shades of color represent the higher confidence levels. The estimated boundaries for the deliquescence zones of 5w, Am-5w, and 7w (through 20w), as well as the 5w–7w phase boundary determined by Kong et al. (2011) are also shown. (b) Estimated stability fields of ferricopiapite (20w), rhomboclase (4w) and paracoquimbite (P9w), plot on the base of final phases of experiments starting with 20w. The darker shades of color represent the higher confidence levels. The estimated boundaries for the deliquescence zones of 20w and 4w are also shown. Legendin plots: 20w = ferricopiapite, 4w = rhomboclase, 5w = $Fe_2(SO_4)_3{\cdot}5H_2O$, 7w = kornelite, Am-5w = amorphous ferric sulfate with five structural water, P9w = paracoquimbite, UK#9 = a hydrous ferric sulfate with distinct Raman spectrum (Fig. 2) of unknown structure, deliq = deliquescence.

7–33% RH and 5–21 °C (Fig. 15a). Defining the exact locations stability fields of a ferric sulfate is dependent on defining all surrounding phase boundaries, such as the study for hexahydrated Mg-sulfate by Chou and Seal (2003).

The low RH side of the stability field of kornelite (7w, Fig. 15a) is defined by the 5w–7w phase boundary, (thin black line, by Kong et al., 2011), while its high RH side is roughly defined by kornelite – ferricopiapite – deliquescence boundary (Section 4.1, red thick line in Fig. 15a). The study of Kong et al. (2011) has not defined the 5w–7w phase boundary below 35.8 °C. The extrapolation (the dotted portion of 5w–7w boundary line in Fig. 15a) is tentative based on the assumption that this boundary intersects with other phase boundaries at low T region. For example, at 21 °C and 54–59% RH, we have observed 7w stayed as 7w, 5w → 5w + 7w + 4w + P9w, Am-5w → 7w + P9w + 4w + 20w, and 20w→20w + 7w→P9w + 20w (Tables 3 and 5–7). These phenomena suggest that 21 °C and 54–59% RH is most likely to be within the stability field of 7w, i.e. it is reasonable to extrapolate the 5w–7w phase boundary down to the vicinity of 21 °C as shown in Fig. 15a. On the other side of this boundary in the range of 7–33% RH and 5–21 °C, the products of six experiments using 7w as starting phase stayed as 7w after 4 years, suggesting either the slow kinetics of dehydration/hydration of 7w prevented the phase transition(s) from occurring (metastable 7w), or an area in this region is within the stability field of 7w but that its boundaries to other ferric sulfates remain unknown. The stability field of 7w probably cannot be extended down to 5 °C (59–64% RH) based on Tables 3, 5 and 7.

The *T*–RH range cycled by 54–59% RH at 21 °C and 59–63% RH at 5 °C is very special (Fig. 15a and b) where paracoquimbite was found in the intermediate and final products of 20 experiments started from all five ferric sulfates (20w, 4w, 5w, 7w, Am-5w). These observations, therefore, indicate the existence of a narrow paracoquimbite stability field in this *T*–RH range (the green colored elliptical zone in Fig. 15a and b). The exact expansion of this stability field as well as its boundaries to other ferric sulfates cannot be defined using the current data. For example, at 63% RH and 5 °C, ferricopiapite stays unchanged, while the transformations of 7w → P9w, 5w → 20w + P9w, 4w → P9w + 20w, Am → 20w + UK#23 were observed. The variety in phase transition at this *T*–RH point can be caused by the rate differences in above phase transition processes or by the expansions of stability fields of involved species. Again, the only way to define the exact location and expansion of paracoquimbite stability field is to determine the locations of all surrounding phase boundaries.

Table 4 shows rhomboclase stayed unchanged in 15 experiments at RH $\leqslant$ 51% within 50–5 °C (with four exceptions related to paracoquimbite and an anhydrous ferric sulfate). It seems that the stability field of rhomboclase could have a wide range with a high RH limit at rhomboclase – deliquescence boundary and a low RH limit at $\leqslant$6% RH and 50 °C where rhomboclase partial dehydrated to an anhydrous ferric sulfate (Figs. 8c and 15b). This stability field may connect to the stability field of paracoquimbite at 54–59% RH 21 °C and at 59–64% RH 5 °C. On the other hand, since the conversion to rhomboclase always happened from ferricopiapite and from Am-5w but almost never from 5w and 7w (whose stability fields at higher temperature, 50–21 °C, known with high confidence), it seems reasonable to assign with high confidence for the zone $\leqslant$21 °C as the stability field of rhomboclase (shown as densely shaded green zone in Fig. 15b), whose high RH side is defined by boundary of deliquescence zone of rhomboclase (thick green line in Fig. 15b).

The dehydration of ferricopiapite was observed during the development of all six experiments at 50 °C with RH $\leqslant$ 65%, which indicates that this region is not within the stability field of ferricopiapite. On the basis of Table 3, we can assign the stability field of ferricopiapite in a wide RH range from 21 °C to 5 °C, which has a high RH limit at the boundary of ferricopiapite – deliquescence, and connects to (or overlap with) the stability field of paracoquimbite at 54–59% RH 21 °C and at 59% RH 5 °C. In addition, three data points at −10 °C (Fig. 15b) tentatively expand the stability field of ferricopiapite to lower temperature range. These data points came from two experiments: (1) a direct RH (79%) measurement (using a Traceable® Hum./Temp/Dew Point meter, No. 4085 from Control Company) of a Fe^{3+}–SO_4–H_2O brine coexisting with ferricopiapite at −10 °C in a sealed container; (2) the stable ferricopiapite structure observed from a sample in an open Petri dish placed in a freezer at −10 ± 1 °C and 62–74% RH (marked by two data point at −10 °C in Fig. 15b) during a period of 4 years. UK#9 phase was observed in the current products of four experiments at 7–11%RH and 21–5 °C started with ferricopiapite. These observations set the low RH limits of the stability field of ferricopiapite, while its exact boundary will be defined by further developments of these experiments and the results from new experiments at −10 °C started a few months ago.

Am-5w stays unchanged in three of the six experiments run at 5–11% RH and at three tested temperatures, 5 °C, 21 °C, and 50 °C, but it re-crystallized to 5w, 6w, 7w, and 4w in other three experiments (Table 7). Between 64–31% (at 50 °C) and 33–64% RH (at 21 °C and 5 °C), Am-5w re-crystallized to variety of ferric sulfates. In addition, at 50 °C and low RH (6–11%), the amorphization of ferricopiapite was observed early in the experiments (20 h), then a UK#9 phase developed and stayed until one year in experiments. The amorphization of ferricopiapite was also observed at two intermediate stages during two experiments run at 7% RH at 21 °C and 5 °C. All these phenomena suggest that the amorphization should be the result of sudden extraction of the structural waters from ferricopiapite. Apparently an amorphous phase can regain the structural ordering within the T range of our experiments. On the basis of these observations, there is no obvious stability field of Am-5w in 50–5 °C and 6–100% RH range.

The finding of a potential stability field of paracoquimbite at mid-RH levels (54–64%) within 21–5 °C range is interesting. Paracoquimbite and ferricopiapite have similar Fe^{3+}:$[SO_4]^{2-}$ ratios and degrees of hydration. In addition, the conversions to paracoquimbite from ferricopiapite (and from all other four ferric sulfates) are very slow, occurring in our experiments after 500–600 days into the reactions at 21 °C (it occurred slightly faster at ~130 days in the experiments of Xu et al. (2009)). These observations argue for a potential overlapping of the stability fields of paracoquimbite and ferricopiapite. A set of experiments at a lower temperature (e.g., −10 °C) may clarify this situation. It is also interesting that paracoquimbite is found to be the conversion product from all tested ferric sulfates in our and Xu's experiment but not coquimbite that is more common in nature. Paracoquimbite has higher numbers of distorted Fe-center octahedral in the structure, i.e. five crystallographically distinct Fe sites, in comparison with three Fe sites in coquimbite. This is probably due to the fact that the *c*-axis of paracoquimbite is three times of that of coquimbite (P9w in Fig. 1). We can anticipate that during a phase transition, a structure with more distortions would first form, while we cannot rule out the possibility of the continuous, slow conversion from paracoquimbite to coquimbite (a less distorted structure) during the development of equilibrium.

4.3. Comparison with previous published studies

The studies by Posnjak and Merwin (1922) and Merwin and Posnjak (1937, and those cited by them) were concentrated on the solid–liquid relationship in a temperature range of 200–50 °C. The data were presented in form of isotherms at 200 °C, 140 °C, 110 °C, 75 °C, and 50 °C, in which the type of minerals (hydrous/anhydrous ferric sulfates, hydroxide and oxide) that precipitate from a brine of certain composition in Fe_2O_3–SO_3–H_2O system were presented. The quadruple points where two ferric sulfates (and/or FeOOH, Fe_2O_3) were found coexisting with a brine (and vapor) were used to construct the phase boundary between these two species in Fe_2O_3–SO_3–H_2O–T ($\leqslant$50 °C) space (Fig. 9 in Posnjak and Merwin (1922)).

Our experimental study reported here concentrated on solid–solid phase transitions in a lower temperature range (50–5 °C) that are more relevant to the current and past Mars surface and subsurface conditions. Our observations that can be compared with those of Posnjak and Merwin (1922) are probably the RH values at 50 °C (the common temperature that both studies used) where the deliquescence of different ferric sulfates occur. The 50 °C data of Posnjak and Merwin (1922) indicated that ferricopiapite or kornelite was found co-existing with brine that has a SO_3:H_2O ratio as ~36:64, while rhomboclase was found co-exiting with the brines with wider SO_3:H_2O ratio (from ~36:64 to 43:57). Like other salts (Greenspan, 1977), these aqueous solutions (saturated or non-saturated) of $Fe_2(SO_4)_3$ can serve as the buffer for relative humidity (RH). In that sense, the observation of Posnjak and Merwin (1922) can be linked to ours. In our observations, the deliquescence of ferricopiapite and kornelite (and crystalline and amorphous 5w) all occurred at 74.4% RH (50 °C), while the deliquescence of rhomboclase happened at a lower RH, i.e., 64.5% (50 °C). The trend that rhomboclase coexists with brine(s) of higher SO3:H_2O ratio than other solid phases in Posnjak and Merwin (1922) observation (their Fig. 8) is consistent with our observation, i.e., its deliquescence occurs at a lower RH level.

A study on the solid–solid phase transitions at room temperature and six RH levels (11–75%), starting with monoclinic and trigonal anhydrous ferric sulfates ((M-$Fe_2(SO_4)_3$ and T-$Fe_2(SO_4)_3$), and aqueous solution of T-$Fe_2(SO_4)_3$, was conducted by Xu et al. (2009), using in situ and ex situ XRD measurements for phase ID. They found the deliquescence of initial anhydrous ferric sulfates at RH >75%, but the initial ferricopiapite with H_2O coating remains unchanged at RH ~62% (controlled by NH_4NO_3 buffer). These results are similar to our observations, i.e., ferricopiapite remains unchanged at RH ~ 70% (KI buffer, 21 °C), while all other four species (4w, 5w, 7w, and Am-5w) became deliquescent at the same RH level. At lower RH (11–33% RH), their observations of the direct precipitation of amorphous phase from solution at low RH(s) is consistent with our work (Fig. 6f). The most interesting agreement is the appearance of paracoquimbite at mid-RH(s) and room temperature: at 53% RH and 22 °C in their experiments (Xu et al., 2009); and at 54–59% RH and 21 °C in our experiments. In addition, the appearance of paracoquimbite is not influenced by the types of starting ferric sulfates in both sets of experiments.

In Fig. 16, we plot the observed solid phases in our experiments (50–5 °C), those from Xu et al. (2009) experiments (at 22 °C), and those from Posnjak and Merwin (1922, at 50 °C) into a SO_3–Fe_2O_3–H_2O ternary diagram. In addition, we add the common hydrous ferric sulfates that were NOT observed in these three experiments in the same plot for evaluation purposes. From these data, we can draw five lines, all started from the H_2O corner of ternary diagram towards Fe_2O_3–SO_3 border. Each line links the mineral species that held a unique ratio of Fe^{3+} to $[SO_4]^{2-}$ with a change in the degree of hydration. For example, The 3rd line from the top represents Fe^{3+}: $SO_4]^{2-}$ = 1:1, and links basic ferric sulfates fibroferrite ($Fe(OH)SO_4{\cdot}5H_2O$) with its dehydration products (butlerite, etc.); the 4th line from the top represents the ferric sulfates with Fe^{3+}:$[SO_4]^{2-}$ = 2:3, and links the normal salts of $Fe_2(SO_4)_3$ with 0, 5, 6, 7, 8, 9, and 10 structural waters per molecule; and the 5th line from the top represents Fe^{3+}:$[SO_4]^{2-}$ = 1:2, and links acidic rhomboclase ($FeH(SO_4)_2{\cdot}4H_2O$) with its dehydration products (one or zero structural water). Notice ferricopiapite in this plot occurs in the space between 3rd and 4th line, i.e., in between the typical normal and basic ferric sulfates. In addition, ferricopiapite does not have hydration or dehydration products that can keep its Fe^{3+}:$[SO_4]^{2-}$ ratio unchanged.

Three of the five starting phases of our 150 experiments occur along the line of normal ferric sulfates (crystalline and amorphous 5w, and 7w, Fe^{3+}: $[SO_4]^{2-}$ ratio = 2:3), plus one acidic (rhomboclase, Fe^{3+}:$[SO_4]^{2-}$ ratio = 1:2) and one basic ferric sulfates (ferricopiapite, Fe^{3+}:$[SO_4]^{2-}$ ratio = 4.67:6). These phases were synthesized from pure chemicals, washed with 98% alcohol several times to remove any residual brine, and their identity and homogeneity were confirmed by XRD on bulk sample along with 100 point Raman measurements. Our experiments placed these species in an environment where only *T* and RH change (i.e. no pH change). A proper hydration or rehydration process should change the mineral phase along one of the lines in Fig. 16, e.g., the hydration/dehydration among normal ferric sulfates with 5w, 7w, and 9w are possible, but the phase transition across different lines should not easily happen. Nevertheless, we have observed cross-line phase transitions in our experiments: such as the transfer of a normal sulfate to a basic or to an acidic sulfates (and verse versa), even from a basic sulfate to an acidic sulfate (i.e., reversible reaction from ferricopiapite to rhomboclase).

The equations of these cross-line phase transitions can be:

Normal to/from basic sulfates (e.g., kornelite and ferricopiapite, Tables 5 and 6)

$$3Fe_2(SO_4)_3\cdot 7H_2O + 8.33H_2O \longleftrightarrow Fe_{4.67}(OH)_2(SO_4)_6\cdot 20H_2O + 1.33FeH(SO_4)_2\cdot 4H_2O + 0.33[HSO_4]^- + 0.33H_3O^+ \tag{1}$$

Acidic to/from normal sulfates (e.g., rhomboclase and paracoquimbite, Table 4)

$$2FeH(SO_4)_2\cdot 4H_2O + 2H_2O \longleftrightarrow Fe_2(SO_4)_3\cdot 9H_2O + H_3O^+ + [HSO_4]^- \tag{2}$$

Acidic to/from basic sulfates (e.g., rhomboclase and ferricopiapite, Table 3)

$$4.67FeH(SO_4)_2\cdot 4H_2O + 6.33H_2O \longleftrightarrow Fe_{4.67}(OH)_2(SO_4)_6\cdot 20H_2O + 3.33[HSO_4]^- + 3.33H_3O^+ \tag{3}$$

These cross-line solid–solid phase transitions involve the change of Fe^{3+}:$[SO_4]^{2-}$ ratio in a solid phase. We believe that can only happen if certain amount of Fe^{3+} or $[SO_4]^{2-}$ was moved out of solid phases. On the basis of Fig. 4a and b, i.e., at mid-high RH levels, thin film of H_2O can form at the surface of a grain (~12.5 extra H_2O/molecule corresponds 2090 layers of H_2O molecules on a 10 μm diameter ferricopiapite grain at 73% RH and 5 °C). This thin film of H_2O can host the ions like Fe^{3+}, $[H_3O]^+$, $[SO_4]^{2-}$, $[HSO_4]^-$, thus change the Fe^{3+}:$[SO_4]^{2-}$ ratios in solid phases and make the cross-line phase transitions (1, 2, 3) possible at those RH levels. Rhomboclase, kornelite, and 5w are less capable than ferricopiapite in holding adsorb H_2O. Based on Figs. 7, 10 and 11, they can hold ~1 extra H_2O/molecule) as compared to ferricopiapite that can hold 6.8–12.5 extra H_2O/molecule at 5 °C, 63–73% RH. This water layer can facilitate the movement of Fe^{3+}, $[H_3O]^+$, $[SO4]^{2-}$, $[HSO_4]^-$ ions. For amorphous ferric sulfates at mid to high RH levels, we observed that the amount of adsorbed H_2O first increased, then Am transformed to crystalline phases (Figs. 12 and 14). During this process, Fe^{3+}, $[H_3O]^+$, $[SO4]^{2-}$, $[HSO_4]^-$ ions can move into inter-grain-liquid and can probably cause the cross-line phase transitions in Fig. 16. During the deliquescence of kornelite and 5w, ferricopiapite was first formed (Eq. (1)), then deliquescence occurred. Nevertheless, no rhomboclase was detected as might be suggested by Eq. (1). It suggests that the term $1.33FeH(SO_4)_2{\cdot}4H_2O$ in right side of Eq. (1) should be in liquid as $1.33(Fe^{3+}+[HSO_4]^{+}+4H_2O)$.

At lower RH levels where a thin film of H_2O may not easily form, extra ions Fe^{3+}, $[H_3O]^+$, $[HSO4]^-$, $[SO4]^{2-}$ can still attach to the broken bonds ($[SO4]^{2-}$ or Fe^{3+}) at a grain surface, or they can simply be

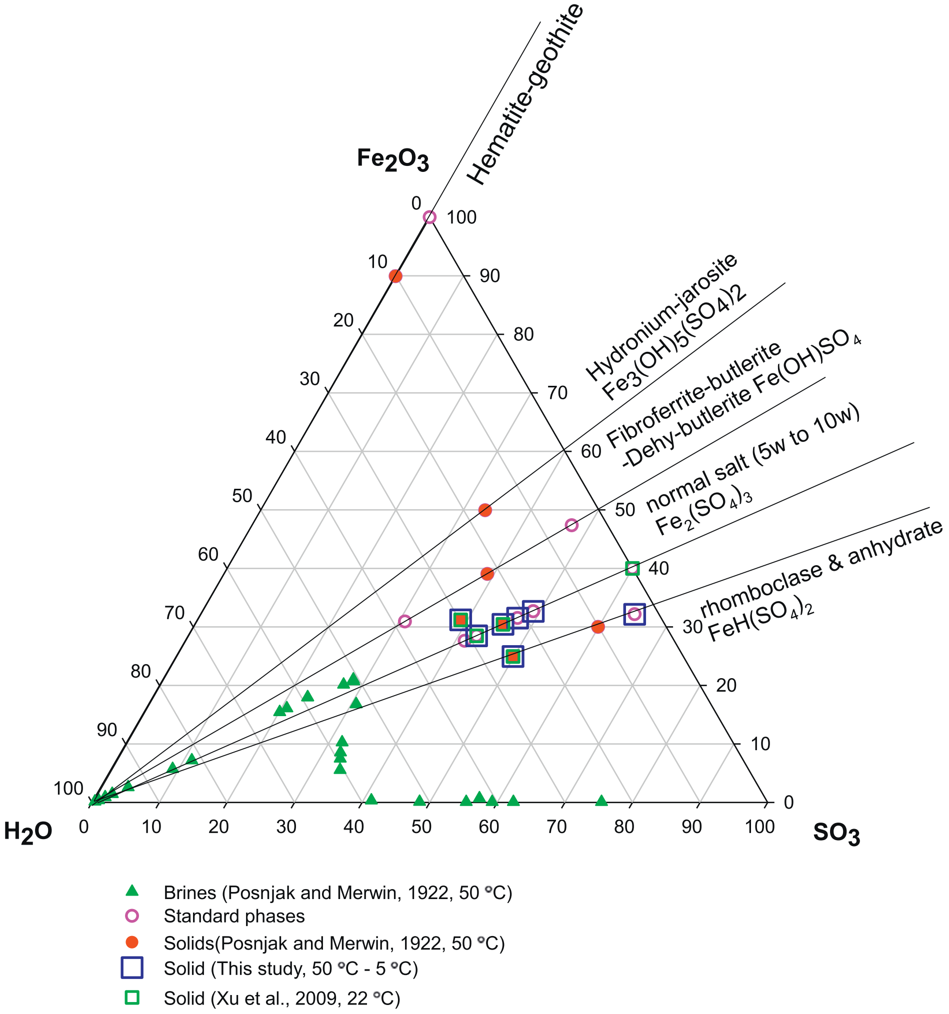

Fig. 16. Ferric sulfates presented in the study of Posnjak and Merwin (1922, at 50 °C), Xu et al., (2009, at 22 °C), and from this work (in 50–5 °C range) in Fe_2O_3–SO_3–H_2O system. Additional standard ferric sulfates, and Fe_2O_3, FeOOH are also plotted. Each straight line connects the ferric sulfates that have a unique Fe to SO_4 ratio but only vary in degree of hydration. Cross-line reactions were observed in the current study with only T and RH as variable experiment conditions.

connected through a hydrogen-bonding. This process of ion adsorption would, however, be less capable in changing the average Fe^{3+}:$[SO_4]^{2-}$ ratio of a solid phase. The probability of cross-line phase transitions would, however, be lower than these at mid-high RH levels. As observed, rhomboclase, kornelite, crystalline and amorphous 5w persisted at RH ⩽33% (Tables 4–7). In contrast, the reversible phase transition between ferricopiapite and rhomboclase happened even at 7% RH and 5 °C, which seems related to the capability of ferricopiapite to hold more water at its grain surface (Fig. 6b and c).

Writing the right side of Eqs. (1)–(3) in a different way may suggest a potential precipitation of FeOOH or $Fe(OH)_3$ during the cross-line phase transitions. Nevertheless, the three-point Raman measurements on each reaction product (and the XRD measurement made by Xu et al. (2009) on bulk sample) were only able to identify the major and minor species. The probability of detecting trace phases such as FeOOH or $Fe(OH)_3$ (weaker Raman scatters than ferric sulfates) was low. In addition, Raman peaks of the ionic species $[SO_4]^{2-}$, $[HSO_4]^{-}$, $[H_2SO_4]^{0}$ in liquid occur very near with those of ferric sulfates, thus the probability of detecting trace amounts of these species would also be low.

The data points of our experiments and those of Xu et al. (2009) in Fig. 16 indicate that there is a limitation on the cross-line phase transitions to happen in the temperature range of our experiments, e.g., no fibroferrite–butlerite and hydronium jarosite (3rd line and 2nd line from the top) or their dehydration products were identified in our (and Xu et al., 2009) reaction products. Nevertheless, because jarosite was identified in Meridiani outcrop on Mars, additional studies on the precipitation conditions of these two types of basic ferric sulfates and their phase transition pathways should also to be conducted.

4.4. Next step – determine the phase boundaries

The results of these experiments (Tables 3–7) place an overall view (although incomplete) of the phase relationships among several normal, basic, and acidic hydrous ferric sulfates, in a wide T–RH space relevant to Mars surface and subsurface conditions (Fig. 15). In order to refine the phase boundaries among them, and especially to build a more detailed understanding of their behaviors on Mars, many follow-up experiments have to be designed and conducted. We have accomplished the determination of a phase boundary between kornelite and pentahydrated ferric sulfate (Kong et al., 2011) using the experimental parameters selected based on this study. The experiments to determine the phase boundary between kornelite (7w), paracoquimbite (P9w), and ferricopiapite (20w) at lower temperatures are planned for future investigations.

4.5. Understanding Mars Iron sulfates

Ferric sulfates were observed on Mars, especially at Gusev and Meridiani sites explored by the Spirit and Opportunity Rovers. With exception of the definitive mineral identification of jarosite (Klingelhofer et al., 2004), most occurrences of iron sulfates in those two sites were determined by Mossbauer spectral analyses to be unspecified ferric sulfates (Morris et al., 2006, 2008), with a few suggested ferric sulfate species based on Vis–NIR spectral deconvolution (Johnson et al., 2007). A special observation was made by the Spirit rover at the Tyrone site in Gusev crater, where a two-layer salty soil was excavated. The lower layer of yellowish-colored salty soil (that was originally buried beneath the surface basic soil and a Ca-sulfate-rich whitish-colored salty soil layer) contains 37% of ferric sulfates, with ferricopiapite as the major component (Johnson et al., 2007). After being exposed to current Mars atmospheric conditions for 198 sols, a color change of yellowish salty soil was observed. In the Vis–NIR spectra extracted from seven systematic multi-color Pancam observations, a reduction of spectral slope from 434 nm to 753 nm was observed from the yellowish Fe-sulfate-rich soil (Wang and Ling, 2011). On the basis of the results presented in this manuscript, especially the occurrence of the dehydration processes from ferricopiapite, we conclude that the phase transitions from ferricopiapite to rhomboclase, Am and quasi-Am are the most likely causes for spectral change in VIS–NIR spectra of Tyrone ferric sulfates.

5. Conclusion

The occurrence of Fe-sulfates on Mars seen by orbital remote sensing is limited in spatial distribution as compared to those of Mg- and Ca-sulfates. Nevertheless, Fe-sulfates are found in surface and subsurface materials at both sites explored by the Spirit and Opportunity Rovers, which emphasizes their importance in martian surface processes involving cycles of S and H_2O. Our systematic experimental investigation of common ferric sulfates under Mars relevant conditions provides the information on their fundamental properties, zones of stability fields, pathways of phase transitions during the changes of hydration degree and acidity, as well as the changes in spectroscopic characteristics of various species occurred during the phase transitions. These results can provide a better understanding of their occurrences and status on Mars and help interpret the science data obtained from the missions to Mars.

Acknowledgments

This investigation was mainly supported by two NASA Mars Fundamental Research Project NNX07AQ34G and NNX10AM89G, partially supported by a NASA Mars Instrument Development project (Contract # 09-030) and NASA MoO Project for ExoMars mission (Contract # 1295053). During their PhD studies at Washington University in St. Louis, Z.C. Ling was supported by a special fund of Shandong University in China, and W.G. Kong was supported by China Scholarship Council. We wish to thank Dr. Z.X. Peng and Ms. Y.L. Lu for their assistance in conducting some Raman, XRD, and gravimetric measurements. We are grateful for two anonymous reviewer whose suggestions have helped the improvement of this manuscript.

References

Ackermann, S., Lazic, B., Armbruster, T., Doyle, S., Grevel, K.D., Majzlan, J., 2009. Thermodynamic and crystallographic properties of kornelite [$Fe_2(SO_4))_3 \sim 7.75H_2O$] and paracoquimbite [$Fe_2(SO_4))_3 9H_2O$]. Am. Mineral. 94, 1620–1628.

Baskerville, W., Cameron, F., 1935. Ferric oxide and aqueous sulfuric acid at 25 °C. J. Phys. Chem. 39, 769–780.

Chiper, S.J., Vaniman, D.T., Bish, D.L., 2007. The effect of temperature and water on ferric sulfates. Lunar Planet. Sci. XXXVIII. Abstract 1409.

Chipera, S.J., Vaniman, D.T., 2007. Experimental stability of magnesium sulfate hydrates that may be present on Mars. Geochim. Cosmochim. Acta. 71, 241–250.

Chipera, S.J., Carey, J.W., Bish, D.L., 1997. Controlled-humidity XRD analyses: Application to the study of smectite expansion/contraction. In: Gilfrich, J. et al. (Eds.), Advances in X-Ray Analysis, vol. 39. Plenum Press, New York, pp. 713–722.

Chou, I.M., Seal, R.R., 2003. Acquisition and evaluation of thermodynamic data for morenosite–retgersite equilibria at 0.1 MPa. Am. Mineral. 88, 1943–1948.

Chou, I.M., Seal, R.R., 2007. Magnesium and calcium sulfate stabilities and the water budget of Mars. J. Geophys. Res. 112, E11004. doi:10.1029/2007JE002898.

Chou, I.M., Seal, R.R., Hemingway, B.S., 2002. Determination of melanterite–rozenite and chalcanthite–bonattite equilibria by humidity measurements at 0.1 MPa. Am. Mineral. 87, 108–114.

Freeman, J.J., Wang, A., Jolliff, B.L., 2007. Pathways to form kieserite from epsomite at mid to low temperatures, with relevance to Mars. Lunar Planet. Sci. Conf. XXXVIII. Abstract 1298.

Freeman, J., Jin, M., Wang, A., 2008. D_2O substitution experiment on hydrated iron and magnesium sulfates and its application for spectral interpretation of martian sulfates. Lunar Planet. Sci. XXXIX. Abstract 2390.

Gellert, R. et al., 2006. Alpha particle X-ray spectrometer (APXS): Results from Gusev crater and calibration report. J. Geophys. Res. 111, E02S05. doi:10.1029/2005JE002555.

Greenspan, L., 1977. Humidity fixed points of binary saturated aqueous solutions. J. Res. Natl. Bureau Stand. A – Phys. Chem. 81A, 89–96.

Hasenmueller, E.A., Bish, D.L., 2005. The hydration and dehydration of hydrous ferric iron sulfates, Lunar Planet. Sci. XXXVI. Abstract 1164.

Haskin, L.A., Wang, A., Jolliff, B.L., McSween, H.Y., Clark, B.C., Des Marais, D.J., McLennan, S.M., Tosca, N.J., Hurowitz, J.A., Farmer, J.D., Yen, A., Squyres, S.W., Arvidson, R.E., Klingelhöfer, G., Schröder, C., de Souza Jr., P.A., Morris, RV., Ming, D.W., Gellert, R., Zipfel, J., Brückner, J.F., Bell III, Herkenhoff, K., Christensen, P.R., Ruff, S., Blaney, D., Gorevan, S., Cabrol, N., Crumpler, A.L., Grant, J., Soderblom, L., 2005. Water alteration of rocks and soils from the spirit rover site, Gusev Crater, Mars. Nature 436, 66–69.

Johnson, J.R. et al., 2007. Mineralogic constraints on sulfur-rich soils from Pancam spectra at Gusev crater. Mars. Geophys. Res. Lett. 34, L13202. doi:10.1029/2007GL029894.

Klingelhofer, G. et al., 2004. Jarosite and hematite at Meridiani Planum from opportunity's Mossbauer spectrometer. Science 306, 1740–1745.

Kong, W.G., Wang, A., Chou, I.M., 2011. Experimental determination of the phase boundary between kornelite and pentahydrated ferric sulfate at 0.1 MPa. Chem. Geol. 284, 333–338.

Lichtenberg, K. et al., 2009. Stratigraphy and relationship of hydrated minerals in the layered deposits of Aram Chaos, Mars. Lunar Planet. Sci. XXXX. Abstract 2326.

Lichtenberg, K.A. et al., 2010. Stratigraphy of hydrated sulfates in the sedimentary deposits of Aram Chaos, Mars. J. Geophys. Res. 15, E00D17. doi:10.1029/2009JE003353.

Ling, Z.C., Wang, A.L., 2010. A systematic spectroscopic study of eight hydrous ferric sulfates relevant to Mars. Icarus. 209, 422–433.

Ling, Z., Wang, A., Jollif, B., Arvidson, R., Xia, H., 2008. A systematic Raman, mid-IR, and vis–NIR spectroscopic study of ferric sulfates and implications for sulfates on Mars. Lunar Planet. Sci. XXXX. Abstract 1463.

Majzlan, J., Botez, C., Stephens, P.W., 2005. The crystal structures of synthetics $Fe_2(SO_4)_3(H_2O)_5$ and the type specimen of lausenite. Am. Mineral. 90, 411–416.

Merwin, H., Posnjak, E., 1937. Sulphate incrustations in the copper Queen mine, Bisbee, Arizona. Am. Mineral. 22, 567–571.

Milliken, R.E., Bish, D.L., 2010. Sources and sinks of clay minerals on Mars. Philos. Mag. 90, 2293–2308.

Milliken, R.E., Fischer, W.W., Hurowitz, J.A., 2009. Missing salts on early Mars. Geophys. Res. Lett. 36, L11202. doi:10.1029/2009GL038558.

Ming, D.W. et al., 2008. Geochemical properties of rocks and soils in Gusev Crater, Mars: Results of the Alpha Particle X-Ray Spectrometer from Cumberland Ridge to Home Plate. J. Geophys. Res. 113, E12S39. doi:10.1029/2008JE003195.

Morris, R.V. et al., 2006. Mossbauer mineralogy of rock, soil, and dust at Gusev crater, Mars: Spirit's journey through weakly altered olivine basalt on the plains and pervasively altered basalt in the Columbia Hills. J. Geophys. Res. 111, E02S13. doi:10.1029/2005JE002584.

Morris, R.V. et al., 2008. Iron mineralogy and aqueous alteration from Husband Hill through Home Plate at Gusev Crater, Mars: Results from the Mossbauer instrument on the Spirit Mars Exploration Rover. J. Geophys. Res. 113, E12S42. doi:10.1029/2008JE003201.

Nordstrom, D.K., Alpers, C.N., 1999. Negative pH, efflorescent mineralogy, and consequences for environmental restoration at the Iron Mountain Superfund site, California. Proc. Natl. Acad. Sci. USA 96, 3455–3462.

Posnjak, E., Merwin, H., 1922. The system, Fe_2O_3–SO_3–H_2O. J. Am. Chem. Soc. 44, 1965–1994.

Roach, L.H. et al., 2009. Testing evidence of recent hydration state change in sulfates on Mars. J. Geophys. Res. 114, E00D02. doi:10.1029/2008JE003245.

Roach, L.H. et al., 2010a. Hydrated mineral stratigraphy of Ius Chasma, Valles Marineris. Icarus 206, 253–268.

Roach, L.H., Mustard, J.F., Lane, M.D., Bishop, J.L., Murchie, S.L., 2010b. Diagenetic haematite and sulfate assemblages in Valles Marineris. Icarus 207, 659–674.

Robinson, P.D., Fang, J.H., 1973. Crystal-structures and mineral chemistry of hydrated ferric sulfates. 3. Crystal-structure of kornelite. Am. Mineral. 58, 535–539.

Smith, M.D. et al., 2004. First atmospheric science results from the Mars Exploration Rovers Mini-TES. Science 306, 1750–1753.

Smith, M.D. et al., 2006. One martian year of atmospheric observations using MER Mini-TES. J. Geophys. Res. 111, E12S13. doi:10.1029/2006JE002770.

Spanovich, N., Smith, M.D., Smith, P.H., Wolff, M.J., Christensen, P.R., Squyres, S.W., 2006. Surface and near-surface atmospheric temperatures for the Mars Exploration Rover landing sites. Icarus. 180, 314–320.

Vaniman, D.T., Chipera, S.J., 2006. Transformations of Mg- and Ca-sulfate hydrates in Mars regolith. Am. Mineral. 91, 1628–1642.

Vaniman, D.T., Bish, D.L., Chipera, S.J., Fialips, C.I., Carey, J.W., Feldman, W.C., 2004. Magnesium sulphate salts and the history of water on Mars. Nature 431, 663–665.

Vaniman, D., Bish, D., Chipera, S., 2009. Bassanite on Mars. Lunar Planet. Sci. XXXX. Abstract 1654.

Wang, A., Ling, Z.C., 2011. Ferric sulfates on Mars: A combined mission data analysis of salty soils at Gusev crater and laboratory experimental investigations. J. Geophys. Res. 116, E00F17. doi:10.1029/2010JE003665.

Wang, A., Freeman, J.J., Jolliff, B.L., Chou, I.M., 2006. Sulfates on Mars: A systematic Raman spectroscopic study of hydration states of magnesium sulfates. Geochim. Cosmochim. Acta. 70, 6118–6135.

Wang, A. et al., 2008. Light-toned salty soils and coexisting Si-rich species discovered by the Mars Exploration Rover Spirit in Columbia Hills. J. Geophys. Res. 113, E12S40. doi:10.1029/2008JE003126.

Wang, A., Freeman, J.J., Jolliff, B.L., 2009. Phase transition pathways of the hydrates of magnesium sulfate in the temperature range 50 °C to 5 °C: Implication for sulfates on Mars. J. Geophys. Res. 114, E04010. doi:10.1029/2008JE003266.

Wang, A., Ling, Z.C., Freeman, J.J., 2010. Stability fields and phase transition pathways of ferric sulfates in 50 °C to 5 °C temperature range. Lunar Planet. Sci. XXXXI. Abstract 2303.

Wang, A., Freeman, J.J., Chou, I.-Ming, Jolliff, B.L., 2011. Stability of Mg-sulfates at −10 °C and the rates of dehydration/rehydration processes under mars relevant conditions. J. Geophys. Res. 116, E12006, doi:10.1029/2011JE003818.

Wirth, F., Bakke, B., 1914. Untersuchung über Ferrisulfate. Darstellung und Eigenschaften der verschiedenen normalen, basischen und sauren Ferrisulfate. Löslichkeitsund Stabilitatsverhaltnisse in Wasser und Schwefelsäure Kristallisationsgang. Zeitschrift fur Anorganische Chemie 87, 13–46.

Xu, W.Q., Tosca, N.J., McLennan, S.M., Parise, J.B., 2009. Humidity-induced phase transitions of ferric sulfate minerals studied by in situ and ex situ X-ray diffraction. Am. Mineral. 94, 1629–1637.